# Collective interactions augment influenza A virus replication in a host-dependent manner

Kara L. Phipps[a], Ketaki Ganti[a‡], Nathan T. Jacobs[a‡], Chung-Young Lee[a‡], Silvia Carnaccini[b], Maria C. White[a], Miglena Manandhar[c], Brett E. Pickett[c†], Gene S. Tan[c,d,f], Lucas M. Ferreri[b], Daniel R. Perez[b,e] and Anice C. Lowen[a,d]*

[a]Department of Microbiology and Immunology, Emory University School of Medicine, Atlanta, Georgia, United States of America

[b]Department of Population Health, Poultry Diagnostic and Research Center, University of Georgia, Athens, Georgia, United States of America.

[c]J. Craig Venter Institute, La Jolla, California, United States of America

[d]Emory-UGA Center of Excellence for Influenza Research and Surveillance (CEIRS), Atlanta, Georgia, United States of America

[e]Center of Research on Influenza Pathogenesis (CRIP) CEIRS, New York, New York, United States of America.

[f]Division of Infectious Disease, Department of Medicine, University of California San Diego, La Jolla, CA, United States of America

[‡]These individuals contributed equally to the research presented.

[†]Present address: Department of Microbiology and Molecular Biology, Brigham Young University, Provo, Utah 84602 USA

*Address correspondence: anice.lowen@emory.edu

**Abstract**

Infection with a single influenza A virus (IAV) is only rarely sufficient to initiate productive infection. Here, we exploit both single-cell approaches and whole-animal systems to show that IAV reliance on multiple infection can form an important species barrier to infection. Namely, we find that H9N2 subtype viruses representative of those circulating widely at the poultry-human interface exhibit acute dependence on collective interactions in mammalian systems. This need for multiple infection is greatly reduced in the natural host. Quantification of incomplete viral genomes showed that their complementation accounts for the more moderate reliance on coinfection seen in avian cells, but not the added reliance seen in mammalian cells. This finding suggests an additional form of virus-virus interaction is needed to support infection in mammalian cells. Genetic mapping implicated the PA gene segment as a major driver of this phenotype and quantification of viral RNA synthesis indicated that both replication and transcription were affected. These findings indicate that multiple distinct mechanisms underlie IAV reliance on multiple infection and underscore the importance of virus-virus interactions in IAV infection, evolution and emergence.

38 **Introduction**

39 Classically, an infectious unit has been defined as a single virus particle which delivers its genome
40 to a cell, initiates the viral reproductive program, and yields progeny viruses. The importance to
41 infection of collective interactions among viruses is being increasingly recognized, however[1-3].
42 The delivery of multiple viral genomes to a cell allows antagonistic and beneficial interactions to
43 occur, and these interactions have the potential to shape transmission, pathogenicity, and viral
44 evolution.

45 Recent work has revealed several distinct mechanisms by which multiple viral genomes
46 are co-delivered to a target cell[4-8]. Various mechanisms of direct cell-to-cell spread yield a similar
47 outcome[9-11]. The implications of multiple infection in these diverse systems are still being
48 explored. In a number of cases, however, collective delivery was demonstrated to increase the
49 efficiency of infection relative to free virus particles[4,5], or to increase the rate of genetic exchange
50 through recombination[6].

51 When distinct variants coinfect, beneficial effects such as compensation of deleterious
52 mutations can increase overall fitness[12-14]. In the case of IAV, several lines of evidence point to a
53 major role in infection for multiplicity reactivation, the process by which segmented genomes
54 lacking one or more functional segments complement each other[15-19]. Conversely, negative
55 interactions can also arise in which deleteriously mutated genes act in a dominant negative
56 fashion. Defective interfering particles, which often potently interfere with the production of
57 infectious progeny from a coinfected cell, are the most extreme example of such antagonism[20-22].

58 Importantly, multiple infection with identical viral genomes can also alter infection
59 outcomes. Such cooperation was documented for VSV and HIV, where rates of transcription and
60 replication were enhanced with increasing multiplicity of infection (MOI)[23,24]. Similarly, faster
61 kinetics of virus production were seen at high MOI for poliovirus and IAV[19,25]. In these instances,
62 it is thought that increased copy number of infecting viral genomes provides a kinetic benefit
63 important in the race to establish infection before innate antiviral responses take hold. Indeed, it

64 has been suggested that multiple infection may be particularly relevant for facilitating viral growth
65 under adverse conditions, such as antiviral drug treatment[3,26].

66 For IAV, an important adverse condition to consider is that of a novel host environment.
67 IAVs occupy a broad host range, including multiple species of wild waterfowl, poultry, swine,
68 humans and other mammals[27,28]. Host barriers to infection typically confine a given lineage to
69 circulation in one species or a small number of related species[29,30]. Spillovers occur occasionally,
70 however, and can seed novel lineages. When a novel IAV lineage is established in humans, the
71 result is a pandemic of major public health consequence[31,32]. The likelihood of successful cross-
72 species transfer of IAV is determined largely by the presence, absence, and compatibility of host
73 factors on which the virus relies to complete its life cycle, and on the viruses' ability to overcome
74 antiviral defenses in the novel host[33-35].

75 Our objective herein was to assess the degree to which IAV relies on the delivery of
76 multiple viral genomes to a cell to ensure production of progeny. In particular, we sought to
77 determine whether this phenotype varies with host species. We therefore examined the
78 multiplicity dependence of one human and a panel of avian-origin viruses in multiple host systems.
79 Results from all virus/cell combinations tested confirm prior reports that cells multiply-infected with
80 IAV produce more viral progeny than singly-infected cells. Importantly, however, the extent to
81 which viral progeny production is concentrated within the multiply-infected fraction of a cell
82 population varies greatly with virus-host context. Two poultry-adapted H9N2 viruses (A/guinea
83 fowl/HK/WF10/99 (GFHK99) and A/quail/HK/A28945/88 (QaHK88)) exhibit an acute dependence
84 on multiple infection in mammalian systems that is greatly diminished in natural host systems.
85 This strong dependence on multiple infection is not seen for the human strain, influenza
86 A/Netherlands/602/2009 (H1N1) (NL09) virus, or for an IAV from wild birds, influenza
87 A/mallard/199106/99 (H3N8) (MaMN99) virus. The host-specific dependence of GFHK99 virus
88 on multiple infection is driven by its PA gene segment. In line with this finding, both bulk and
89 single-cell measurements of viral RNA showed that polymerase activity in mammalian cells is

90 enhanced with multiple infection. A need for complementation of incomplete viral genomes
91 partially accounts for this cooperative effect. Importantly, however, single-cell data indicate that
92 additional multiplicity-dependent mechanisms support RNA synthesis by the GFHK99 virus in
93 mammalian cells. Thus, our data point to an important role for multiple infection in determining
94 the potential for IAV replication in diverse hosts.
95
96 **Results**
97 ***Degree of multiplicity dependence varies with strain and cell type***
98 To evaluate the extent to which IAV relies on multiple infection for productive infection, we
99 initially used reassortment and coinfection as readouts. While singly infected cells yield only
100 parental progeny, reassortment is highly efficient within coinfected cells[36]. Monitoring
101 reassortment therefore indicates the proportion of progeny in a bulk virus population that were
102 produced from multiply infected cells. To ensure accurate quantification of reassortment,
103 coinfections were performed under single-cycle conditions with homologous viruses that differ
104 only by a silent mutation in each segment and the presence of either an HA or HIS epitope tag
105 fused to the HA protein. The silent mutations allow identification of reassortant viruses. The
106 epitope tags enable quantification of cellular coinfection across a range of MOIs. Homologous
107 coinfection partners, termed WT and VAR, were generated in NL09, MaMN99 and GFHK99 strain
108 backgrounds.
109 Coinfection and reassortment were examined in canine MDCK and chicken DF-1 cells
110 (**Figure 1**). In MDCK cells, GFHK99 viruses showed a near linear relationship between total $HA^+$
111 cells and dual-$HA^+$ cells, suggesting a strict dependence on multiple infection for HA expression
112 (**Figure 1A**). By contrast, HA expression resulting from infection with a single strain was more
113 common for GFHK99 in DF-1 cells, MaMN99 in MDCK cells and NL09 in MDCK cells (**Figure**
114 **1A**). To give a quantitative measure of the differences among these virus/cell pairings, we
115 determined the degree of linearity from the regression models of each dataset (**Figure 1B**). The

116 more dependent expression of *any* HA protein is on coinfection, the more linear the relationship
117 between dual-HA$^+$ cells and HA$^+$ cells becomes. Conversely, a relationship closer to the Poisson
118 expectation indicates less dependence on coinfection. Among the viruses tested, we found that
119 only GFHK99 virus in MDCK cells exhibits strong linearity in the relationship between HA$^+$ and
120 dual-HA$^+$ cells (**Figure 1B**).

121 In line with observed levels of coinfection, GFHK99 virus exhibits high levels of
122 reassortment in MDCK cells, indicating that nearly all progeny virus is produced from WT-VAR$_1$
123 coinfected cells (**Figure 1C**). MaMN99 or NL09 viruses infecting MDCK cells show relatively lower
124 levels of reassortment. Moreover, reassortment of GFHK99 viruses is markedly reduced in DF-1
125 cells compared to MDCK cells (**Figure 1C**). These results clearly reveal differing degrees of
126 multiplicity dependence for different virus/cell pairings and therefore indicate that multiple infection
127 dependence is determined through virus-host interactions.

128 That all virus-cell pairings tested show evidence of multiplicity dependence is highlighted
129 by comparison of the experimental reassortment data to a theoretical prediction (**Figure 1C**). This
130 theoretical prediction was published previously[18] and is derived from a computational model in
131 which the number of viral progeny produced by an infected cell is constant, irrespective of the
132 number of input viral genomes. Because singly- and multiply-infected cells make equivalent
133 numbers of progeny in this model, reassortment is predicted to increase only gradually at low
134 levels of infection where coinfection is relatively rare. The experimental observation that
135 reassortment reaches high levels much more rapidly than expected indicates that viral progeny
136 production is enriched in the proportion of the infected cell population that is multiply infected.

137 Frequent reassortment and the linear relationship between overall HA expression and HA
138 co-expression provide two measures of multiplicity dependence for a given virus-cell pairing. To
139 summarize these two measures and analyze the relationships between the virus-cell pairings
140 tested, we conducted a hierarchical clustering analysis using the parameters of the regression
141 models shown in **Figure 1A** and **1C**. MaMN99 and NL09 viruses in MDCK cells, as well as

142 GFHK99 virus in DF-1 cells, represent one cluster, while GFHK99 virus in MDCK cells partitioned
143 into its own cluster (**Figure 1D**). Coinfection dependence, therefore, is evident in all virus-cell
144 pairings, but particularly strong for GFHK99 virus in MDCK cells.
145
146 ***Strain- and host-specific phenotypes are also evident* in vivo**
147 To determine whether host-dependent reliance on multiple infection extended to *in vivo*
148 models, we performed coinfections in guinea pigs and quail. GFHK99, MaMN99, and NL09
149 viruses were tested in guinea pigs and GFHK99 virus was examined in quail. To ensure use of
150 comparable effective doses for each virus/host pairing, the 50% infectious dose ($ID_{50}$) of each
151 virus mixture was first determined experimentally in the animal models used. Guinea pigs were
152 then infected intranasally with $10^2$ $GPID_{50}$ of each WT/VAR mixture and nasal washes were
153 collected daily. Quail were infected with $10^2$ $QID_{50}$ of the GFHK99 virus mixture via an oculo-naso-
154 tracheal route and tracheal swabs were collected daily. To evaluate the frequency of
155 reassortment, plaque isolates from these upper respiratory samples were genotyped for each
156 animal on each day. Because multicycle replication *in vivo* allows the propagation of reassortants,
157 analysis of genotypic diversity rather than percent reassortment is more informative for these
158 experiments. Thus, the effective diversity (Hill's $N_2$) was calculated for each dataset and plotted
159 as a function of time post-inoculation (**Figure 1E, 1F**). The viruses collected from GFHK99-
160 infected guinea pigs show much higher genotypic diversity throughout the course of infection than
161 viruses isolated from MaMN99- or NL09-infected guinea pigs (**Figure 1E**) or GFHK99-infected
162 quail (**Figure 1F**). These data indicate that the virus-host interactions which determine
163 dependence on multiple infection in cell culture extend to *in vivo* infection.
164
165 ***Multiple infection enhances viral growth***
166 The abundant reassortment observed with GFHK99 viruses in mammalian systems
167 suggests that multiple infection plays a major role in determining the productivity of an infected

168 cell. We therefore hypothesized that increasing MOI would augment the viral output of infected
169 cells and that the magnitude of this effect would be greater for GFHK99 virus in MDCK cells than
170 for GFHK99 virus in DF-1 cells or MaMN99 and NL09 viruses in MDCK cells. To test this
171 prediction, we infected over a range of MOIs and then measured PFU produced per cell under
172 single-cycle conditions. The input MOIs for this series of experiments were based on PFU as
173 determined in MDCK cells. Which MOI conditions were saturating was determined empirically by
174 flow cytometry in MDCK and DF-1 cells (**Supplementary Figure 1**). MOIs < 1 PFU/cell were
175 found to be non-saturating. Under these non-saturating conditions, increasing MOI resulted in
176 accelerated viral growth and higher burst size for all virus/cell pairings (**Figure 2A–D**). As
177 predicted, however, increasing the MOI of GFHK99 virus in MDCK cells resulted in a further
178 enhancement of viral amplification (**Figure 2G**). Thus, the benefit conferred by multiple infection
179 was greater for GFHK99 virus in MDCK cells compared to the other virus-cell pairings tested.
180 We reasoned that the cooperative effect observed might result from i) complementation
181 of incomplete viral genomes or ii) a benefit of increased viral genome copy number per cell. In an
182 effort to differentiate between these possibilities, we measured growth of GFHK99 virus in MDCK
183 and DF-1 cells infected over range of saturating MOIs. Note that plaque assays in MDCK cells
184 underestimate the infectious potential of GFHK99 virus, and increasing viral MOI beyond 1
185 PFU/cell did not lead to increased levels of HA+ cells, indicating saturation (**Supplementary**
186 **Figure 1**). Under these conditions, incomplete viral genomes are unlikely to be prevalent and any
187 benefit of increasing MOI would be attributable to increasing genome copy numbers per cell. In
188 both cell types, MOIs between 1 and 20 PFU per cell result in similar peak viral titers (**Figure 2E,**
189 **F, H**). This saturation of cooperation at higher MOIs suggests diminishing returns from additional
190 genome copies above a certain threshold. Whether this threshold is imposed by a need for
191 complementation or another mechanism sensitive to saturation remained unclear.
192
193 ***Multiple infection enhances viral RNA replication***

194 To test whether multiple infection was beneficial to the virus at the level of genome
195 replication, we measured WT viral RNA synthesis in the absence and presence of increasing
196 amounts of a homologous coinfecting virus. We also broadened the panel of viruses examined to
197 include two additional strains: A/duck/HK/448/78 (H9N2) (DkHK78), a wild bird isolate that
198 predates the establishment of H9N2 viruses in poultry, and A/quail/HK/88 (H9N2) (Qa/HK/88), an
199 early isolate of the H9N2 poultry lineage[37]. To evaluate host specificity, we measured WT viral
200 RNA synthesis in both mammalian and avian cells (**Figure 3**). Cells were infected with low MOI
201 of WT virus to ensure receipt of a single copy of the WT virus genome. Concurrently, cells were
202 infected with increasing doses of a VAR virus. Droplet digital PCR (ddPCR) was then used to
203 quantify replication of WT genomes using primer/probe sets that do not detect VAR templates.
204 The results for NL09 and MaMN99 viruses show little to no increase in WT vRNA
205 production with VAR virus addition, in all cell types tested (**Figure 3A and B**). DkHK78 virus
206 exhibits an intermediate phenotype, with up to 7-fold increases in WT vRNA levels seen with VAR
207 virus addition in MDCK and NHBE cells. For this virus in avian DF-1 cells, only a 1.6-fold increase
208 is observed (**Figure 3C**). GFHK99 and QaHK88 viruses show much stronger enhancement of WT
209 vRNA replication with VAR virus coinfection: in MDCK and NHBE cells, respectively, GFHK99
210 virus show increases of 60-fold and 20-fold, while QaHK88 virus shows increases of more than
211 2000-fold and 200-fold. In contrast, these two poultry isolates show markedly less enhancement
212 in WT vRNA replication with VAR coinfection in avian DF-1 cells (**Figure 3D and E**). Of note,
213 addition of VAR at high doses suppresses WT vRNA production in several virus/cell pairings,
214 likely indicating competition for limited resources in the cell. This antagonistic interaction is
215 stronger in systems where little benefit of coinfection is detected.
216 In summary, for both GFHK99 and QaHK88 viruses, the introduction of coinfecting VAR
217 virus reveals a cooperative effect acting at the level of RNA synthesis, which is particularly potent
218 in mammalian cells. That the replication of NL09 and MaMN99 viruses is not detectably enhanced

219 by the addition of VAR virus suggests a reduced reliance on multiple infection, consistent with
220 reassortment and dual-HA positivity data presented above.
221
222 ***The viral PA segment is a major determinant of multiple infection dependence***
223 To identify viral genetic determinants of multiple infection dependence, we mapped
224 segments responsible for the high reassortment phenotype of GFHK99 virus in MDCK cells. One
225 or more genes from GFHK99 virus was placed into a MaMN99 virus background. For each
226 chimeric genotype, WT and VAR strains were generated to allow tracking of homologous
227 reassortment. Coinfections were performed in MDCK cells and HA expression and reassortment
228 were measured as in **Figure 1**. Two viruses are similar to the parental GFHK99 virus in the levels
229 of dual HA positivity observed: MaMN99:GFHK99 3PNP and MaMN99:GFHK99 PA (**Figure 4A–**
230 **B**). Quantification of reassortment revealed that several chimeric viruses reassort at a higher
231 frequency than MaMN99 parental strains, but that the MaMN99:GFHK99 3PNP and
232 MaMN99:GFHK99 PA viruses show the highest reassortment, comparable to that seen for the
233 parental GFHK99 genotype (**Figure 4C-D**). A clustering analysis similar to the one shown in
234 **Figure 1D** revealed that only these two genotypes cluster with GFHK99 parental virus, while each
235 of the other genotypes clusters with MaMN99 virus (**Figure 4E**). Thus, while other viral genes
236 may contribute, PA is the primary genetic determinant of the high reassortment exhibited by
237 GFHK99 virus in MDCK cells and defines a need for cooperation between coinfecting viruses. To
238 verify the contribution of the PA segment by a second approach, we evaluated the impact of VAR
239 virus coinfection on WT vRNA synthesis for the MaMN99:GFHK99 PA chimeric strain in MDCK
240 and DF-1 cells. The results confirm that the PA segment of GFHK99 virus increases reliance on
241 multiple infection, specifically in mammalian cells (**Supplementary Figure 2**).
242
243 ***Multiple infection accelerates viral replication and transcription***

244 Because mapping of the GFHK99 high reassortment phenotype implicated the viral PA,
245 we tested the effects of multiple infection on viral replication and transcription by measuring vRNA
246 and mRNA over time following low or high MOI infection (**Figure 5**). GFHK99 virus was examined
247 in DF-1 and MDCK cells and MaMN99 virus was tested in MDCK cells. To ensure viral genomes
248 were supplied as low or single copies, a dose of 0.5 RNA copies per cell was used for low MOI
249 infection. Under these low MOI conditions in MDCK cells, GFHK99 genomic RNA levels remain
250 low throughout the time course. GFHK99 mRNA increases early, perhaps reflecting robust
251 primary transcription, then accumulates at a relatively slow rate from 2 h post-infection onward
252 (**Figure 5A**). Both viral RNA species accumulate at a significantly higher rate for GFHK99 virus
253 in DF-1 cells and MaMN99 virus in MDCK cells (**Figure 5B, C, G**). For the high MOI dose, we
254 used 3.0 HA-expressing units per cell, as determined by flow cytometry (**Supplementary Figure**
255 **3**). This measure of infectivity gives a functional readout for polymerase activity, and therefore
256 ensures the vast majority of cells carry an active viral polymerase. At this high MOI, accumulation
257 of GFHK99 mRNA and vRNA in MDCK cells occurs at a similar rate to that seen for GFHK99
258 virus in DF-1 cells or MaMN99 virus in MDCK cells (**Figure 5D–F, H**). Thus, a host-specific defect
259 in GFHK99 polymerase activity that affects both replication and transcription is seen at low MOI.
260 This defect is, however, resolved under conditions where multiple infection is prevalent.
261

262 ***Single-cell mRNA sequencing reveals a need for cooperation***

263 To evaluate the heterogeneity of viral RNA synthesis at the single-cell level, we infected DF-1 or
264 MDCK cells with GFHK99 virus under single-cycle conditions and collected cells at 8 h post-
265 infection for mRNA barcoding on the 10x Genomics Chromium platform prior to sequencing. Cells
266 in which no viral mRNA was detected were excluded from further analysis. In addition, we used
267 a thresholding approach to exclude cells that were unlikely to be truly infected, but rather may
268 carry small amounts of viral mRNA owing to lysis of neighboring cells (**Supplementary Figure**
269 **4**). Following these two exclusion steps, the number of cells remaining ranged between 110 and

270 440 per infection condition. Next, to allow comparison between cell types and between
271 experiments, each cell's total transcript abundance was normalized to the median number of
272 transcripts per cell in the relevant sample. The normalized and $\log_{10}$ transformed counts of viral
273 transcripts per cell were then compared across conditions. We found that the amount of detected
274 GFHK99 viral mRNA varies widely between individual DF-1 cells, which is consistent with
275 previous observations[38-40]. In contrast, GFHK99 viral mRNA levels are uniformly low in MDCK
276 cells, especially at the lower MOIs tested (**Figure 6A**, left facet).

277 To evaluate whether low transcript abundance corresponded with the failure to detect one
278 or more polymerase-encoding segments, we stratified the data based on detection of all four
279 segments necessary to support transcription (PB2, PB1, PA and NP). Consistent with prior
280 reports[38], viral transcript levels are higher in cells that contained PB2, PB1, PA, and NP transcripts
281 compared to those in which one or more of these transcripts was not detected (**Supplementary**
282 **Figure 5**). We noted that the PB2, PB1, and PA mRNAs were markedly less abundant than the
283 other viral transcripts, however. Thus, the correspondence between failure to detect polymerase
284 transcripts and low viral mRNA abundance may simply be due to the higher likelihood of these
285 mRNAs falling below the limit of detection in cells that have low overall viral transcription.

286 To measure the impact of coinfecting viruses in individual cells, we repeated the single-
287 cell sequencing experiment with the addition of two variants of GFHK99 virus, GFHK99 $mVAR_1$
288 and GFHK99 $mVAR_2$. Cells were inoculated with GFHK99 WT and GFHK99 $mVAR_1$ viruses in a
289 1:1 ratio. Coinfection with GFHK99 $mVAR_2$ virus was performed simultaneously and this virus
290 was used at the concentration found to give optimal support of WT viral RNA replication in **Figure**
291 **3D**: 0.1 PFU per cell in DF-1 cells and 1.0 PFU per cell in MDCK cells. After mRNA sequencing,
292 only cells in which transcripts from all eight $mVAR_2$ virus segments were detected were analyzed
293 further. Cells that likely obtained WT or $mVAR_1$ viral RNA through lysis were excluded
294 (**Supplementary Figure 4**). Between 64 and 217 cells per infection condition met both criteria to
295 be included in further analysis. As expected, no significant difference was detected between WT

296 and $mVar_1$ transcript levels ($p > 0.05$, linear mixed effects model) (**Supplementary Figure 5**). No
297 differentiation is therefore made between strains in further analysis. In cells infected with both WT
298 and $mVAR_1$ viruses, viral transcript abundance is calculated separately for each, so that
299 coinfected cells contribute two distinct measurements to the dataset. The viral transcript levels
300 per cell detected in this second experiment are shown in **Figure 6A** alongside data from the first
301 experiment. In comparing the two infections, we observe that total viral transcript abundance is
302 markedly lower in MDCK cells compared to DF-1 cells in the first infection, but this effect is almost
303 entirely mitigated by the presence of $mVAR_2$ virus in the second infection. This reduction in the
304 disparity between DF-1 and MDCK cells resulted from the fact that $mVAR_2$ virus increased
305 transcript abundance by 149% in DF-1 cells, but 258% in MDCK cells ($p < 10^{-4}$, linear mixed
306 effects model) (**Figure 6A)**. These data underscore the significance of viral collective interaction
307 to ensure productive infection in diverse hosts.

308 Because only a subset of a cell's transcripts is captured and therefore reliably detected[41],
309 the 10x platform does not allow a robust determination of segment presence or absence in a cell.
310 The addition of $mVAR_2$ virus improves the sensitivity with which WT transcripts can be detected,
311 however, and – as noted above – levels the playing field between MDCK and DF-1 cells. We
312 therefore evaluated the number of distinct viral gene segments detected per cell, as indicated by
313 the presence of the corresponding mRNAs. Failure to detect a subset of the eight segments in a
314 given cell is very common in our datasets, as with others[38,40]. The addition of $mVAR_2$ virus
315 increases the number of segments per cell detected, however, suggesting that failure to detect is
316 often a result of transcript levels falling below the limit of detection of the assay (**Figure 6B**).
317 Importantly, in the presence of $mVAR_2$ virus, the number of segments detected per cell was
318 comparable between MDCK and DF-1 cells across all MOIs tested (**Figure 6B**). This result
319 suggests that the frequency with which incomplete GFHK99 viral genomes are expressed is
320 comparable between these mammalian and avian cell lines.
321

322 ***Frequency of incomplete GFHK99 genomes in MDCK cells is moderate***

323 Given the limitations of single-cell mRNA sequencing for the detection of relatively rare
324 transcripts, we employed a second single-cell approach to quantify the frequency with which fewer
325 than eight vRNAs are replicated in GFHK99 infected MDCK cells[19]. MDCK cells were coinfected
326 with a low MOI of GFHK99 WT virus and a high MOI of GFHK99 $VAR_2$ virus. The GFHK99 $VAR_2$
327 virus acts to ensure propagation of the WT virus gene segments, even when less than the full WT
328 viral genome is available for transcription and replication. Following inoculation, single cells were
329 sorted into wells which contain a naïve cell monolayer and multicycle replication was allowed for
330 48 h. To determine which viral gene segments were present in the initially sorted cell, RT-qPCR
331 with primers that differentiate WT and $VAR_2$ gene segments was applied. As detailed in the
332 Methods, the results were used to calculate the probability that a cell infected with a single WT
333 virus contains a given segment. We termed the resultant parameter Probability Present ($P_P$). The
334 experimentally determined $P_P$ values vary among the segments, with a range of 0.56 to 0.8
335 (**Figure 7A**). The product of the eight $P_P$ values gives an estimate of the proportion of singular
336 infections in which all eight segments are available for replication. This estimate is 3.2% for
337 GFHK99 virus in MDCK cells.

338 To evaluate whether incomplete viral genomes account for the focusing of GFHK99 virus
339 production within multiply infected cells, we used our previously published computational model
340 of IAV coinfection and reassortment[18]. In this model, the frequency of successful segment
341 replication is governed by eight $P_P$ parameters and an infected cell only produces virus if at least
342 one copy of all eight segments are replicated. Importantly, in this model the amount of virus
343 produced from productively infected cells is constant – there is no additional benefit to multiple
344 infection. When the eight experimentally determined $P_P$ values for GFHK99 virus in MDCK cells
345 are used to parameterize the model, the theoretical prediction of reassortment frequency is much
346 lower than that observed experimentally for GFHK99 viruses in MDCK cells, but a good match
347 with the reassortment seen in DF-1 cells (**Figure 7B**). Clearly, the frequency with which GFHK99

348 segments fail to be replicated cannot fully account for the high reassortment seen in the
349 mammalian MDCK cell system, but can fully account for the more moderate reliance on multiple
350 infection seen in DF-1 cells. Thus, in mammalian cells, a full GFHK99 viral genome is necessary
351 but not sufficient to support robust replication.
352
353 **Discussion**
354 Our data reveal that moderate reliance of IAV on multiple infection is the norm. An exceptionally
355 high need for multiple infection can, however, occur when an IAV infects a new host species.
356 Thus, our findings identify increased reliance on multiple infection as a novel component of IAV
357 host restriction. Since not all mismatched virus-host combinations show a high reliance on
358 multiple infection, the data indicate that a need for collective interactions is a potential
359 manifestation of IAV host restriction, not a universal feature. Dependence on multiple infection is
360 of particular interest as a barrier to cross-species transfer for two reasons: first, it can be overcome
361 in the absence of genetic adaptation, through high dose infection; and second, it leads to high
362 levels of reassortment, which in turn can facilitate adaptation to a new host.
363 An important consequence of viral genome segmentation is the potential for replication of
364 incomplete genomes[2]. Complementation is therefore a major class of collective interaction for
365 viruses with segmented genomes. The relevance of complementation for a given virus species
366 likely depends on the extent to which packaging, delivery and replication of genome segments is
367 coordinated[42]. For IAV, we and others have demonstrated that a subset of segments fails to be
368 replicated or expressed in infected cells with high frequency[16,19,38,40]. Specifically, for influenza
369 A/Panama/2007/99 (H3N2) virus in MDCK cells, we found that delivery of a single viral genome
370 results in replication of all eight segments only 1.2% of the time[19]. Data reported herein for
371 GFHK99 virus indicate that a somewhat higher proportion of replicated viral genomes are
372 complete – namely, 3.2%. Thus, GFHK99 virus is partially dependent on complementation for
373 productive infection. However, the high levels of reassortment seen between GFHK99 WT and

374 VAR viruses in mammalian cells indicate that additional cooperative interactions are at play. This
375 is clear from the discrepancy between observed GFHK99 virus reassortment in MDCK cells and
376 the reassortment levels expected if complementation is the only cooperative effect considered.
377 These data point to a model in which the presence of not just complete genomes, but rather
378 multiple copies of the viral genome, are needed to overcome host-specific barriers to GFHK99
379 infection in mammalian systems (**Figure 8**).

380 Insight into the nature of this second cooperative interaction is gleaned from the
381 observation that the amount of viral RNA produced from GFHK99 WT viral genomes is
382 significantly increased with the addition of a homologous virus. From these data, we can conclude
383 that the coinfecting virus functions in *trans* to support WT virus RNA replication in mammalian
384 cells. In addition, our genetic data implicate the viral PA in defining an acute reliance on
385 cooperation. The PA gene segment encodes two proteins: PA and PA-X[43]. Together with PB2
386 and PB1, PA is an essential component of the trimeric polymerase complex[44]. PA carries the
387 endonuclease activity required for cap-snatching from nascent Pol II transcripts, which is essential
388 for viral transcription[45]. It also comprises much of the interface for viral polymerase dimerization,
389 which is needed for viral replication[46]. PA-X shares its N-terminus with PA but has a unique 41 or
390 61 amino acid C-terminus[43,47]. PA-X contributes to the shut-off of host protein synthesis by
391 targeting host Pol II transcripts for destruction[48,49]. Alignment of PA and PA-X proteins encoded
392 by GFHK99 and MaMN99 viruses reveals 29 differences in PA and 9 differences in PA-X
393 (**Supplementary Figure 6**). Three-dimensional modeling of the GFHK99 and MaMN99 PA
394 proteins based on the recently reported structure of the A/NT/60/1968 (H3N2) virus polymerase[46]
395 did not predict marked differences. Nevertheless, the polymorphisms noted in and near the
396 dimerization loop suggest a model in which the reliance of GFHK99 virus on multiple infection
397 may result from an inefficiency of polymerase dimerization and consequent inefficiency of vRNA
398 synthesis[46]. This model is attractive based on the results of Fan et al., who reported that aberrant
399 *in vitro* initiation of vRNA synthesis by a dimerization mutant was ameliorated with increased

400 polymerase concentration[46]. We speculate that multiple infection could lead to a similar effect
401 within the infected cell. If this speculation is correct, it would suggest a role for host factors in viral
402 polymerase dimerization, since the observed GFHK99 reliance on multiple infection is specific to
403 mammalian cells. Finer mapping of the phenotype within PA and targeted functional studies are
404 needed to test this model and explore other possible mechanisms.

405 Of note, high reliance on multiple infection in mammalian cells does not extend to all avian
406 IAVs. Our experiments indicate that this phenotype is a feature of H9N2 subtype avian IAV
407 prevalent at the poultry-human interface, while two avian IAV derived from wild birds, MaMN99
408 and DkHK78 viruses, showed no increase or a modest increase in reliance on multiple infection
409 in mammalian relative to avian systems. Whether a need for multiple infection in mammalian cells
410 extends to other poultry-adapted lineages is an interesting question for future study. H9N2
411 subtype viruses are, however, highly relevant in the context of zoonotic infection due to their
412 prevalence at the poultry-human interface. Sporadic human infections with poultry-adapted H9N2
413 viruses have been reported, including with strains closely related to GFHK99 virus. These H9N2
414 viruses furthermore share several related genes with H5N1 and H7N9 subtype viruses that have
415 caused hundreds of severe human infections[50-55]. The G1 lineage to which the GFHK99 virus
416 belongs circulates widely in the poultry of Southeast Asia, the Middle East, and North Africa and
417 reassorts frequently with other poultry adapted IAVs[56-59]. Our comparison of reassortment in
418 guinea pigs and quail indicates that reassortment could be particularly prevalent in the context of
419 zoonotic infection of mammals. This phenotype of high reassortment in mammals is expected to
420 extend to the H5N1 and H7N9 subtype viruses of public health concern, which carry polymerase
421 genes related to those of the GFHK99 virus[53-55]. While reassortment is typically deleterious[60,61],
422 high frequencies increase opportunity for fit genotypes to arise and adapt, and should therefore
423 be considered in assessing the risk of emergence posed by non-human adapted IAVs.

424 Our data reveal novel concepts in both virus-host and virus-virus interactions. In the
425 context of virus-host interactions, the extent of IAV reliance on cooperation is determined in part

426 by interactions with the host cell, such that infection of novel hosts may be characterized by an
427 acute dependence on multiple infection. In the context of virus-virus interactions, our data show
428 that cooperation is not limited to complementation; rather, interactions among homologous
429 coinfecting viruses can be highly biologically significant. Viral dependence on multiple infection is
430 expected to have a strong impact on viral fitness and evolution by modulating the efficiency of
431 spread within and between hosts and by changing how a virus population samples sequence
432 space[62-65]. Thus, multiple infection dependence is likely to play an important role in determining
433 the outcomes of IAV infection and evolution in diverse hosts.
434

435 **Acknowledgements**

436 We thank David Stallknecht (University of Georgia) for providing the A/mallard/MN/199106/99
437 (H3N8) biological isolate. We thank Hui Tao, Shamika Danzy, and Ginger Geiger for technical
438 assistance. This work was funded in part by NIH R01 AI127799 (to ACL and DRP); NIH/NIAID
439 Centers of Excellence in Influenza Research and Surveillance (CEIRS), contract numbers
440 HHSN272201400004C (to ACL and GST) and HHSN272201400008C (to DRP). Additional funds
441 were provided by the Georgia Research Alliance and the Georgia Poultry Federation (to DRP)
442 and NIH/NIAID Genomic Centers for Infectious Diseases (GCID), Award Number U19AI110819.
443

444 **Author Contributions**

445 KLP contributed to the conception of work, experimental design, data acquisition and analysis,
446 interpretation of data; KG, NTJ and C-YL contributed to experimental design, data acquisition and
447 analysis and interpretation of data; SC contributed to data acquisition; MM and MCW contributed
448 to data acquisition and analysis; BEP contributed to data analysis and interpretation; GST
449 contributed to conception of the work, data analysis and interpretation; LMF contributed to data
450 acquisition; DRP contributed to experimental design, data analysis and interpretation; ACL

451 contributed to conception of work, experimental design and data analysis and interpretation. All
452 authors contributed to the writing of the manuscript.
453
454 **Conflict of interest statement**
455 The authors declare no conflicts of interest.
456
457 **Data availability**
458 10x Genomics single-cell sequencing data is available on the GEO database with the accession
459 number XXXXXXXX. Other data are available from the corresponding author upon reasonable
460 request.
461
462 **Code availability**
463 Code used for 10x Genomics analysis is available at:
464 https://github.com/njacobs627/GFHK99_Multiplicity. Code used to run the agent-based model on
465 influenza A virus reassortment was reported previously[18,19] and is also available at
466 https://github.com/njacobs627/GFHK99_Multiplicity.
467
468 **Methods**
469 ***Cells and cell culture media***
470 Madin-Darby canine kidney (MDCK) cells, a gift from Peter Palese, Icahn School of Medicine at
471 Mount Sinai, were used in all experiments. MDCK cells from Daniel Perez at University of Georgia
472 were used for plaque assays as this variant of the MDCK line was found to yield more distinct
473 plaques for the GFHK99 strain. Both MDCK cell lines were maintained in minimal essential
474 medium (MEM; Gibco) supplemented with 10% fetal bovine serum (FBS; Atlanta Biologicals),
475 penicillin (100 IU), and streptomycin (100 µg per mL) (PS; Corning). 293T cells (ATCC CRL-3216)

476 and DF-1 cells (ATCC CRL-12203) were maintained in Dulbecco's minimal essential medium
477 (DMEM; Gibco) supplemented with 10% FBS and PS. Duck embryo cells (ATCC CCL-141) were
478 maintained in Eagle's minimum essential medium (EMEM; ATCC) supplemented with 10% FBS
479 and PS. Normal human bronchial epithelial (NHBE) cells were acquired from Lonza and were
480 amplified and differentiated into air-liquid interface cultures as recommended by Lonza and
481 described by Danzy et al.[66]. All cells were cultured at 37°C and 5% $CO_2$ in a humidified incubator.
482 Medium for culture of IAV in each cell line (virus medium) was prepared by supplementing the
483 appropriate media with 4.3% bovine serum albumin and penicillin (100 IU), and streptomycin (100
484 µg per mL). Ammonium chloride-containing virus medium was prepared by the addition of HEPES
485 buffer and $NH_4Cl$ at final concentrations of 50 mM and 20 mM, respectively.
486
487 ***Viruses***
488 All viruses were generated by reverse genetics[67]. For avian viruses, 293T cells transfected with
489 reverse genetics plasmids 16–24 h prior were injected into the allantoic cavity of 9–11 day old
490 embryonated chicken eggs and incubated at 37°C for 40–48 h. The resultant egg passage 1
491 stocks were used in experiments. For NL09-based viruses, 293T cells transfected with reverse
492 genetics plasmids 16–24 h prior were co-cultured with MDCK cells at 37°C for 40–48 h.
493 Supernatants were then propagated in MDCK cells from low MOI to generate NL09 working
494 stocks. Defective interfering segment content of PB2, PB1, and PA segments was confirmed to
495 be minimal for each virus stock, as described previously[68] (**Supplementary Figure 7)**. All plaque
496 assays were performed in MDCK cells; viruses were also titered by flow cytometry and/or RT
497 qPCR-based methods where indicated. The reverse genetics system for influenza A/guinea
498 fowl/Hong Kong/WF10/99 (H9N2) virus was reported previously[69,70]. This strain has been referred
499 to as WF10 in previous publications[69-71]. For consistency with other strains used in the present
500 manuscript, it is referred to herein as GFHK99. A low passage isolate of influenza
501 A/mallard/Minnesota/199106/99 (H3N8) virus, referred to herein as MaMN99, was obtained from

502 David Stallknecht at the University of Georgia[72]. The virus was passaged once in eggs and then
503 the eight cDNAs were generated and cloned into the pDP2002 vector[73]. A low passage isolates
504 of influenza A/duck/Hong Kong/448/1978 (H9N2) and A/quail/Hong Kong/A28945/1988 (H9N2),
505 referred to herein as dkHK78 and QaHK88, were passaged once in eggs and then the eight
506 cDNAs were generated and cloned into the pDP2002 vector. To increase the recovery efficiency
507 of viruses containing polymerase components from the MaMN99 virus, pCAGGS support
508 plasmids encoding PB2, PB1, PA, and NP proteins of the A/WSN/33 (H1N1) strain were supplied.
509 GFHK99 WT, MaMN99 VAR and NL09 VAR viruses were engineered to contain a 6XHis
510 epitope tag plus GGGS linker at the N-terminus of the HA protein following the signal peptide.
511 GFHK99 $VAR_1$, MaMN99 WT and NL09 VAR viruses contain similarly modified HA genes, with
512 an HA epitope tag plus a GGGS linker inserted at the N-terminus of the HA protein[36]. All assays
513 except the single-cell mRNA sequencing used viruses carrying these epitope tags.
514 Silent mutations were introduced into VAR viruses by site-directed mutagenesis to allow
515 genotyping of WT and VAR segment origin. The specific changes introduced into all VAR viruses
516 used here are listed in **Supplementary Table 1.** Mutations introduced into GFHK99 $VAR_1$,
517 MaMN99 VAR, and NL09 VAR viruses enable detection by high-resolution melt analysis or probe-
518 based droplet digital PCR. Mutations introduced into the GFHK99 $VAR_2$ strain were designed to
519 confer unique primer binding sites relative to GFHK99 WT virus. Viruses used for single-cell
520 mRNA sequencing, GFHK99 $mVAR_1$ and GFHK99 $mVAR_2$, carry mutations near the 3' end of
521 each transcript to allow detection by sequencing following oligo-dT priming[38].
522
523 ***Synchronized, single-cycle infection conditions***
524 Conditions designed to synchronize viral entry and prevent propagation of progeny viruses were
525 used for all cell culture-based infections with the exception of those performed for measurement
526 of $P_P$ values. Synchronized, single-cycle infections were performed as follows: Cell monolayers
527 were washed three times with PBS and placed on ice. Chilled virus inoculum was added to each

528 well and incubated at 4°C for 45 minutes with occasional rocking to allow attachment without
529 entry[74]. Inoculum was aspirated and cell monolayer was washed three times with cold PBS before
530 addition of warm virus medium lacking trypsin. Cultures were incubated at 37°C. At 3 h post-
531 infection, virus medium was replaced with ammonium chloride-containing virus medium. Addition
532 of ammonium chloride to the medium prevents acidification of endosomes, thereby blocking
533 further IAV infection[75]. Cultures were returned to 37°C for the remainder of the incubation time.
534

535 ***Infection of cultured cells for quantification of coinfection and reassortment***

536 MDCK or DF-1 cells were seeded at a density of 4 x$10^5$ cells per well in 6-well dishes 24 h before
537 inoculation. Virus inoculum was prepared by combining WT and VAR viruses at high titer in a 1:1
538 ratio based on PFU titers, and then diluting in PBS to achieve MOIs ranging from 10 to 0.01 PFU
539 per cell. Synchronized, single cycle infection conditions were used. In addition, owing to the low
540 yield of IAV in DF-1 cells, acid inactivation of inoculum virus was performed at 1 h post-infection
541 for this cell type. This procedure is needed if residual inoculum virus would otherwise comprise
542 an appreciable proportion of the virus sampled at 12 or 16 h post-inoculation. For acid inactivation,
543 media was aspirated and replaced with 500 µL of PBS-HCl, pH 3.00 and incubated 5 min at 37°C.
544 Cells were then washed once with PBS before the addition of virus medium. GFHK99 virus-
545 infected cells were harvested at 12 h post-infection due to high amounts of cytopathic effects at
546 later time points. Cells infected with MaMN99 virus and MaMN99:GFHK99 chimeric viruses were
547 harvested at 16 h post-infection. NL09 virus reassortment data shown in Figure 1C were reported
548 previously[76] and are included here to allow comparison to the avian strains used.
549

550 ***Determination of infection and coinfection levels based on HA surface expression.*** To
551 enumerate infected cells, surface expression of HIS and HA epitope tags was detected by flow
552 cytometry (**Supplementary Figure 8**). This method was previously described in detail[36]. Cells
553 were fixed following staining by resuspending in FACS buffer and 1% paraformaldehyde. The

554 percentage of cells positive for either or both epitope tags is expressed as % cells $HA^+$. The
555 percentage of cells positive for both epitope tags is expressed as % cells dual-$HA^+$. The
556 relationship between these two parameters was evaluated by plotting % cells dual-$HA^+$ against %
557 cells $HA^+$ and regressing the resultant curve as a polynomial:

558 $$\%\ cells\ dual\text{-}HA^+ = \beta_2 * \text{Expectation}(\%\ cells\ HA^+) + \beta_1 * (\%\ cells\ HA^+),$$

559 where $\beta_2$ and $\beta_1$ are genotype-specific. For a given fraction of cells expressing HA, the expected
560 fraction of cells expressing both HA proteins is derived from the Poisson distribution with
561 $\lambda = -ln(1 - \%\ cells\ HA^+)$:

562 $$\sum_{v=1}^{\infty} \frac{e^{-\lambda}\lambda^v}{v!}(1 - 2 * 0.5^v)$$

563

564 From the regression models, we then quantified the degree of linearity using the equation:

565 $$\%\ linearity = \frac{|\beta_1|}{|\beta_1| + |\beta_2|}.$$

566

567 ***Animal models and reassortment* in vivo**

568 Ethics Statement. All animal experiments were conducted in accordance with the Guide for the
569 Care and Use of Laboratory Animals of the National Institutes of Health. Studies were conducted
570 under animal biosafety level 2 (ABSL-2) containment and approved by the IACUC of the
571 University of Georgia (protocols A201506-026-Y3-A2 and A201506-026-Y3-A5) for quail studies
572 or the IACUC of Emory University (protocol PROTO201700595) for guinea pig studies. Animals
573 were humanely euthanized following guidelines approved by the American Veterinary Medical
574 Association (AVMA).

575 Quail eggs obtained from the College of Veterinary Medicine, University of Georgia, were
576 hatched at the Poultry Diagnostic and Research Center, University of Georgia. Two days before
577 virus inoculation, quail sera were confirmed to be seronegative for IAV exposure by NP ELISA

578 (IDEXX, Westbrook, ME). At 3 weeks of age, birds were moved into a HEPA in/out BSL2 facility
579 and each group divided into individual isolator units.

580 Groups (n=6) of 3 week old Japanese quail (Coturnix Japonica) were used to determine
581 the 50% quail infectious dose of the 1:1 GFHK99 WT and GFHK99 $VAR_1$ virus mixture. Each
582 quail was inoculated with 500 µl by oculo-naso-tracheal route of virus mixture in PBS, at
583 increasing concentrations of $10^0$ to $10^6$ $TCID_{50}$ per 500 µL. Tracheal and cloacal swab specimens
584 were collected daily from each bird in brain heart infusion media (BHI). Swab samples were
585 analyzed by $TCID_{50}$ assay and titers of tracheal swabs collected at 4 d post-inoculation were used
586 to determine the $QID_{50}$ by the Reed and Muench method[77]. Virus was not detected in cloacal
587 swabs. $QID_{50}$ was found to be equivalent to 1 $TCID_{50}$.

588 To quantify reassortment in quail, samples collected from quail (n=6) infected with the $10^2$
589 $TCID_{50}$ dose of the 1:1 GFHK99 WT and GFHK99 $VAR_1$ virus mixture were used. These were the
590 same birds as used to determine $QID_{50}$. Virus shedding kinetics were determined by plaque assay
591 of tracheal swab samples and samples from days 1, 3, and 5 were chosen for genotyping of virus
592 isolates.

593 Female Hartley strain guinea pigs weighing 250–350 g were obtained from Charles River
594 Laboratories (Wilmington, MA) and housed by Emory University Department of Animal
595 Resources. Prior to intranasal inoculation and nasal washing, guinea pigs were sedated by
596 intramuscular injection with 30 mg per kg ketamine/ 4 mg per kg xylazine. The $GPID_{50}$ of GFHK99
597 WT/$VAR_1$ and MaMN99 WT/VAR virus mixtures were determined as follows. Groups of four
598 guinea pigs were inoculated intranasally with virus mixture in PBS at doses of $10^0$ to $10^5$ PFU per
599 300 µL inoculum. Daily nasal washes were collected in 1 mL PBS and titered by plaque assay.
600 Results from day 2 nasal washes were used to determine the $GPID_{50}$ by the Reed and Muench
601 method[77]. The $GPID_{50}$ of GFHK99 virus was found to be 2.1 x $10^3$ PFU; that of MaMN99 virus
602 was 2.1 x $10^1$ PFU. The GPID50 of NL09 virus was previously determined to be 1 x $10^1$ PFU (ref[78]
603 and data not shown).

604 To evaluate reassortment kinetics in guinea pigs, groups of six animals were infected with
605 $10^2$ x $GPID_{50}$ of the aforementioned GFHK99 WT / $VAR_1$, MaMN99 WT / VAR or NL09 WT / VAR
606 virus mixtures. Virus inoculum was given intrasnasally in a 300 µL volume of PBS. Nasal washes
607 were performed on days 1–6 post-inoculation and titered for viral shedding by plaque assay. HRM
608 genotyping was performed on samples collected on day 1, 3, and 5 for each guinea pig.
609
610 ***Quantification of reassortment and effective diversity***
611 Reassortment was quantified for *in vitro* coinfection supernatants, guinea pig nasal washes, and
612 quail tracheal swabs as described previously[36]. Briefly, plaque assays were performed in 10 cm
613 dishes to isolate virus clones. 1 mL serological pipettes were used to collect agar plugs into 160
614 µl PBS. Using a ZR-96 viral RNA kit (Zymo), RNA was extracted from the agar plugs and eluted
615 in 40 µl nuclease free water (Invitrogen). Reverse transcription was performed using Maxima RT
616 (Thermofisher) according to the manufacturer's protocol. The resulting cDNA was diluted 1:4 in
617 nuclease free water and each cDNA was combined with segment specific primers
618 (**Supplementary Table 2**) and Precision Melt Supermix (Bio-Rad) and analyzed by qPCR in a
619 CFX384 Touch real-time PCR detection system (Bio-Rad) designed to amplify a ~100 bp region
620 of each gene segment which contains a single nucleotide change in the VAR virus. The qPCR
621 was followed by high-resolution melt (HRM) analysis to differentiate WT and VAR amplicons[79].
622 Precision Melt Analysis software (Bio-Rad) was used to determine the parental virus origin of
623 each gene segment based on melting properties of the cDNAs and comparison to WT and VAR
624 controls. Each individual plaque was assigned a genotype based on the combination of WT and
625 VAR genome segments, with 2 variants on each of 8 segments allowing for 256 potential
626 genotypes.
627 Reassortment data was used to calculate viral genotypic diversity; that is, the diversity of
628 the 256 possible WT/VAR genotypes present in a given sample. Diversity was quantified as
629 reported previously[80], by calculating Simpson's Index, given by $D = \text{sum}(p_i^2)$, where $p_i$ represents

630 the proportional abundance of each genotype[81]. Simpson's Index accounts for both the raw
631 number of species and variation in abundance of each, and is sensitive to the abundance of
632 dominant species. These features are important to ensure that overrepresentation of a single
633 reassortant genotype does not cause a viral population to appear more diverse than it actually is.
634 Because Simpson's Index does not scale linearly, each sample's Simpson's Index value was
635 converted to a corresponding Hill number to derive its effective diversity, $N_2 = 1/D$[82], which is
636 defined as the number of equally abundant species required to generate the observed diversity
637 in a sample community. Because it scales linearly, Hill's $N_2$ allows a more intuitive comparison
638 between communities (i.e., a community with $N_2 = 10$ species is twice as diverse as one with $N_2 =$
639 5) and is suitable for statistical analysis by basic linear regression methods[83]. Robust linear
640 models of $N_2$ vs. time were regressed using the R package *robustlmm*.
641

642 ***Hierarchical clustering analysis***

643 To compare the behavior of multiple viruses during *in vitro* coinfections, a hierarchical clustering
644 algorithm was used. In these experiments, multiplicity dependence was measured by analyzing
645 HA co-expression and reassortment as a function of the percentage of cells expressing HA. Each
646 of these regression models contain two parameters ($\%\ cells\ dual\text{-}HA^+ = \beta_2 *$ Expectation($\%\ cells$
647 $HA^+$) + $\beta_1 *(\%\ cells\ HA^+)$, and $\%\ reassortment = \beta_0 + \beta_1 * ln(\%\ cells\ HA^+)$. The behavior of a given
648 virus can therefore be expressed as a set of four parameters. These parameters were used to
649 calculate the distance between each pair of viruses, and Ward's method of aggolomerative
650 hierarchial clustering was then used to organize viruses into clusters based on these distances[84].
651 Briefly, this algorithm combines a nearby pair of elements into a cluster with a new position that
652 is halfway between the original individuals. This process is repeated until all elements have been
653 incorporated into one cluster. The R package *pvclust* was used to calculate statistical support for
654 the existence of each node by multiscale bootstrap resampling, with nodes appearing in 95% of

655 trials being deemed statistically significant. Each dendrogram was then divided into two clusters
656 to determine whether the behavior of GFHK99 virus in MDCK cells represented a true outgroup
657 (**Figure 1**), or to determine whether each GFHK99:MaMN99 chimeric virus was more similar to
658 GFHK99 or MaMN99 parent virus (**Figure 4**).
659
660 ***Single-cycle viral growth kinetics***
661 DF-1 or MDCK cells were seeded at $4x10^5$ cells per well in 6 well dishes 24 h prior to infection.
662 Virus was serially diluted using PBS. Synchronized, single cycle infection conditions with acid
663 inactivation of inoculum virus as described above were used. At each time point, 120 µl
664 supernatant was collected. Viral titers for each sample were assessed by plaque assay in MDCK
665 cells. Each MOI condition was used in 5–6 wells in parallel infections. Three wells served as
666 technical replicates for growth curve sampling while the remaining wells were harvested at 24 h
667 post-infection to enumerate HA-expressing cells via flow cytometry. Flow cytometry data for NL09
668 in MDCK cells are not included owing to low sensitivity of the assay for this virus. In cases where
669 acid inactivation was inefficient, the replicate was eliminated, and data are plotted in duplicate.
670
671 ***Effect of increasing multiple infection on viral RNA replication***
672 For DF-1 and MDCK cell experiments, 12-well plates were seeded with $3x10^5$ cells per well 24 h
673 prior to infection. For NHBE cells, cells were cultured at an air-liquid interface as previously
674 described[66]. Cell surfaces were washed three times with PBS prior to inoculation. Triplicate wells
675 were then inoculated with increasing doses of VAR virus, plus 0.005 PFU per cell of WT virus in
676 DF-1 and MDCK cells or 0.05 PFU per cell of WT virus in NHBE cells. VAR viruses used were
677 GFHK99 $VAR_2$, MaMN99 VAR, NL09 VAR, MaMN99-Anhui-PA VAR, MaMN99-GFHK99-PA
678 VAR, dkHK78 VAR, and QaHK88 VAR. After 55 minutes at 37°C, inoculum was aspirated, cells
679 were washed three times with PBS and 1 ml per well virus medium was added. Media was
680 exchanged for ammonium chloride-containing media 3 h later. At 12 h post-infection, virus media

681 was removed and cells were harvested using RNAprotect Cell Reagent (Qiagen). RNA was
682 extracted using RNeasy columns (Qiagen) and then reverse transcribed with universal influenza
683 primers[85] and Maxima RT per protocol instructions. Droplet digital PCR (ddPCR) was performed
684 on the resultant cDNA. For GFHK99 virus, QX200™ ddPCR™ EvaGreen Supermix (Bio-Rad)
685 was used with a combination of PB2, M, and NS primers specific for the GFHK99 WT virus (final
686 primer concentration of 200 nM) (**Supplementary Table 3**). For MaMN99, MaMN99-Anhui-PA,
687 MaMN99-GFHK99-PA, dkHK78, QaHK88 and NL09 viruses, QX200™ ddPCR™ Supermix for
688 Probes (Bio-Rad) was used with NP specific primers and probes (**Supplementary Table 3**).
689
690 ***Strand-specific quantification of viral RNA species over time***
691 Viruses used for this experiment were the same GFHK99 WT/$VAR_1$ or MaMN99 WT/VAR
692 virus mixtures used to measure reassortment, but in this case each mixture was considered as a
693 single virus population (i.e. the RT ddPCR assay outlined below to quantify viral m/vRNA does
694 not differentiate between WT and VAR genotypes). Doses used were 0.5 RNA copies per cell for
695 the low MOI and 3.0 HA-expressing units/cell for the high MOI. RNA copy numbers of virus stocks
696 were determined by ddPCR targeting at least four segments (mean values were used). HA-
697 expressing units per mL was determined by counting $HA^+$ cells by flow cytometry in the relevant
698 cell type. Specifically, cells were infected with serial dilutions of virus under synchronized, single
699 cycle conditions. At 24 h post-infection, cells were harvested and flow cytometry was performed
700 targeting His and HA epitope tags. HA expressing units per mL for each virus / cell combination
701 was calculated based on the linear range of $\%HA^+$ cells plotted as a function of volume of virus
702 added to cells[86] (**Supplementary Figure 3**).
703 12-well plates were seeded with $2x10^5$ cells per well of MDCK or DF-1 cells and incubated
704 at 37°C for 24 h. Synchronized, single cycle infection conditions were used, as described above.
705 Chilled virus was added at a volume of 125 µL per well. At 0, 1, 2, 4, 6, 8, and 10 h post-infection,
706 virus medium was aspirated and cells were harvested using 400 µL of RNAprotect Cell Reagent

707 (Qiagen). RNA was extracted using the Qiagen RNAeasy Mini kit. Two reverse transcription
708 reactions per sample were set up with primers targeting mRNA or vRNA of the NS segment, each
709 containing different nucleotide barcode tags (**Supplementary Table 4**). Maxima RT was used
710 according to the manufacturer's instructions and combined with 300 ng MDCK or 150 ng DF-1
711 RNA. Absolute copy number of cDNA was determined by ddPCR. Forward and reverse primers
712 for vRNA or mRNA of NS at a total concentration of 200 nM were combined with diluted cDNA
713 and QX200™ ddPCR™ EvaGreen Supermix (Bio-Rad). Primer sequences are given in
714 **Supplementary Table 4**. Thermocycler protocol was 95°C for 5 min, [95°C for 30s, 57°C for 60s]
715 repeat 40x, 4°C for 5 min, 90°C for 5 min, 4°C hold. Copy number was normalized to RNA input
716 to give final results in units of copy number per ng RNA. We did attempt to measure cRNA in this
717 assay but found that primers designed to be specific for cRNA cross-primed on viral mRNA.
718
719 ***Single-cell mRNA sequencing***
720 For this assay, viruses were titered in DF-1 cells using flow cytometry with anti-NP antibody. DF-
721 1 cells were used because they give more sensitive detection of GFHK99 virus infection than
722 MDCK cells. Cells were infected with serial dilutions of virus under synchronized, single-cycle
723 conditions. At 24 h post-infection flow cytometry was performed targeting NP: cells were
724 processed with the BD Cytofix/Cytoperm™ Kit (catalog no. 554714) and stained with anti-NP
725 antibody (Abcam, clone 9G8, catalog no. ab43821) followed by donkey anti-Mouse IgG Alexa
726 Fluor 488 (Invitrogen catalog no. A-21202). NP expression units per were calculated based on
727 the linear range of % cells $NP^+$ plotted as a function of volume of virus added to cells[86]
728 (**Supplementary Figure 3**).
729 To perform single-cell mRNA sequencing, MDCK and DF-1 cells were seeded into 6-well
730 plates at $5x10^5$ cells per well. At 24 h post seeding, cells were infected with synchronized, single
731 cycle conditions. In the first experiment, MDCK or DF-1 cells were inoculated with GFHK99 WT
732 virus at an MOI of 0.07, 0.2, 0.6, or 1.8 NP units per cell. In the second experiment, MDCK or DF-

733 1 cells were inoculated with a 1:1 ratio of GFHK99 WT virus and GFHK99 $mVAR_1$ virus that
734 amounted to a MOI of 0.02, 0.07, 0.2 or 0.6 NP units per cell. GFHK99 $mVAR_2$ virus was added
735 to MDCK and DF-1 cell infections at MOIs of 1 PFU per cell and 0.1 PFU per cell, respectively.
736 Infected cells were incubated for 8 h at 37°C. Culture media was then aspirated and cells washed
737 once with 1X PBS. Cells were then trypsinized with 200 µL of 0.25% Trypsin EDTA until all cells
738 came off the plate and were mono-dispersed. To each well, 0.5 mL of virus medium was added
739 and replicates were pooled (2 wells per MOI). Cells for each sample were counted. Samples were
740 spun at 150 rcf for 3 minutes and washed with 0.5 mL of 1X PBS/0.04% BSA. Washings were
741 performed two more times. Finally, cells were resuspended with 1X PBS/0.04% BSA to give 7 x
742 $10^5$ cells per mL. Preparation for single-cell transcriptomic sequencing followed the protocol for
743 10x Genomics Chromium Single Cell platform.

744 Analysis of viral transcripts from single cells was performed with the sequencing data from
745 all experiments using Cell Ranger software. Briefly, the Cell Ranger software assigns each read
746 to individual cells and transcripts based on two sets of unique molecular identifiers (UMIs) that
747 are ligated prior to amplification. This approach allows the quantification of amplification bias at
748 both the cellular and transcript levels. The first step of the analytical workflow was to map the
749 reads to concatenated transcriptomes of GFHK99 virus with the transcriptomes of dog or chicken
750 to analyze MDCK and DF-1 cell infections, respectively. Protein coding regions for the dog and
751 chicken transcriptomes were identified in the GTF file associated with genome builds
752 CanFam3.1.98 (NCBI accession number GCA_000002285.2) and GRCg6a (NCBI accession
753 number GCA_000002315.5), respectively, while GFHK99 virus coding regions were extracted
754 from the reverse-complement sequences of the GFHK99 strains. The aligned sequencing data is
755 available on the GEO database with the accession number XXXXXXXX. Cell Ranger output in
756 the form of gene and barcode counts were then analyzed in R using the package *CellrangerRkit*.
757 To account for the issue of cellular lysis, which can allow uninfected cells to acquire viral RNA

758 from the supernatant and thus appear infected, a preliminary analysis was conducted to exclude
759 cells that were likely false positives. This analysis was informed by the reasoning that 1)
760 contaminated cells were likely to contain less viral RNA than truly infected cells, and 2) the amount
761 of viral RNA present in contaminated cells should be less consistent than the amount present in
762 truly infected cells. Within each infection, the proportion of each cell's transcriptome that was
763 comprised of viral RNA was calculated, and cells were ordered according to this proportion so
764 that the marginal gain in % viral RNA from one cell to the next could be calculated. Excluding cells
765 with no marginal gain (indicating two cells with the same % viral RNA), the marginal gain vs. %
766 viral RNA was plotted for each infection, which showed that this marginal gain is initially a rapidly
767 decreasing function of % viral RNA. The first local minimum of a local regression was derived for
768 each infection, to determine the point at which marginal gain became more consistent and less
769 affected by % viral RNA, and cells with % viral RNA below that threshold were excluded from
770 further analysis (**Supplementary Figure 4**). To enable comparisons between samples, the
771 median number of UMIs per cell was calculated for each infection, and the UMI counts of each
772 cell within that infection were normalized to this median value (e.g. if the total number of UMIs in
773 a cell was 50% of that detected in the median cell, all of its UMI counts were multiplied by 2). The
774 number of viral RNA transcripts per cell was then calculated and $\log_{10}$-transformed.
775
776 ***Single-cell sorting assay for measurement of $P_P$ values***
777 Segment-specific $P_P$ values were determined as previously described for influenza
778 A/Panama/2007/99 (H3N2) virus[19], and as follows. $4 \times 10^5$ MDCK cells were seeded into each well
779 of a 6-well dish. 24 h later, cells were washed 3x with PBS and inoculated with 0.018 PFU per
780 cell of GFHK99 WT virus and 1 PFU per cell of GFHK99 $VAR_2$ virus in 250 µL of PBS. Virus was
781 allowed to attach at 37°C for 1 h. Inoculum was then removed and cells were rinsed 3x with PBS
782 and 2 mL of virus medium was added to the well. After 1 h at 37°C, medium was removed and
783 cells were washed 3x with PBS and harvested by addition of Cell Dissociation Buffer (Corning).

784 Cells were resuspended in complete medium and washed 3x with 2 mL FACS buffer (2% FBS in
785 PBS). A final resuspension step was performed in PBS containing 1% FBS, 10 mM HEPES, and
786 0.1% EDTA. Cells were strained through a cell strainer cap (Falcon) and sorted on a BD Aria II
787 cell sorter. Gating was performed to remove debris and multiplets and one event per well was
788 sorted into each well of a 96-well plate containing MDCK monolayers at 30% confluency in 50 µl
789 virus medium supplemented with 1 ug per mL TPCK-treated trypsin. Following the sort, an
790 additional 50 µl of virus medium plus TPCK-treated trypsin was added to each well and plates
791 were centrifuged at 1,800 rpm for 2 minutes to promote cell attachment. Plates were incubated at
792 37°C for 48 h to allow propagation of virus from the sorted cell.

793 RNA was extracted from infected cells in the 96-well plate using a ZR-96 Viral RNA Kit
794 (Zymo Research) per manufacturer instructions. Extracted RNA was converted to cDNA using
795 universal influenza primers[85] and Maxima RT according to manufacturer instructions. After
796 conversion, cDNA was diluted 1:4 with nuclease-free water and used as template (4 µL per
797 reaction) for segment-specific qPCR using SsoFast EvaGreen Supermix (Bio-Rad) in 10 µl
798 reactions, with 200 nM final primer concentration. Primers employed targeted each segment of
799 GFHK99 WT virus, as well as the PB2 and PB1 segments of GFHK99 $VAR_2$ virus. Primer
800 sequences are listed in **Supplementary Table 3**.

801 Given the MOI of GFHK99 WT virus used in the experiments, an appreciable number of
802 wells are expected to receive two or more viral genomes, and so a mathematical adjustment is
803 needed to estimate the probability of each genome segment being delivered by a single virion.
804 Using the relationship between MOI and the fraction of cells infected from Poisson statistics, i.e.,
805 $f = 1 - e^{-\mathrm{MOI}}$, the probability of the *i*th segment being present in a singly infected cell, or $P_{P,i}$ can
806 be calculated from the 96-well plate using the following equation:

807
$$P_{P,i} = \frac{\mathrm{MOI}_i}{\mathrm{MOI}_{\mathrm{wt}}} = \frac{-\ln\,(1 - f_i)}{-\ln\,(1 - f_{\mathrm{wt}})} = \frac{\ln\,(1 - \frac{C_i}{A})}{\ln\,(1 - \frac{B}{A})}$$

808 where $A$ is the number of $VAR_2^+$ wells, $B$ is the number of $WT^+$ wells (containing any WT segment),

809 and $C_i$ is the number of wells positive for the WT segment in question. Wells that were negative

810 for $VAR_2$ virus segments were excluded from analysis.

811 **Figure Legends**

812 **Figure 1. Coinfection and reassortment frequencies indicate that IAV multiplicity**
813 **dependence varies with virus strain and host species.** A–D) MDCK or DF-1 cells were
814 coinfected with homologous WT and VAR viruses of either GFHK99, MaMN99, or NL09 strain
815 backgrounds at a range of MOIs. The relationship between % cells $HA^+$ and % cells dual-$HA^+$ (A)
816 varies with strain and cell type, resulting in curves of differing % linearity (B). GFHK99, MaMN99,
817 and NL09 viruses exhibit different reassortment levels in MDCK cells, but all show high
818 reassortment relative to a theoretical prediction in which singly infected and multiply infected cells
819 have equivalent burst sizes (C). GFHK99 virus reassortment levels differ in MDCK and DF-1 cells,
820 but again reassortment in DF-1 cells remains high relative to the theoretical prediction in which
821 multiple infection confers no advantage (C). Clustering analysis of reassortment and HA co-
822 expression regression models determines that GFHK99 virus exhibits unique behavior in MDCK
823 cells compared to DF-1 cells or other viruses in MDCK cells (D). Yellow circles indicate nodes
824 with >95% bootstrap support. In guinea pigs (n=6), GFHK99 WT and $VAR_1$ viruses exhibit higher
825 reassortment than MaMN99 or NL09 WT and VAR viruses, as indicated by increased genotypic
826 diversity (E). The GFHK99 WT and $VAR_1$ viruses exhibit higher reassortment in guinea pigs than
827 in quail (n=5) (F). Guinea pig data shown in panels E and F are the same. NL09 virus reassortment
828 data shown in (C) were reported previously[76]. Shading represents 95% CI.

829

830 **Figure 2. Increasing MOI increases viral productivity at sub-saturating, but not saturating**
831 **MOIs.** MDCK or DF-1 cells were infected under single-cycle conditions at a range of MOIs in
832 triplicate wells for each MOI. A–F) Viral titers observed at the indicated MOIs are plotted against
833 time post-infection for GFHK99 virus in MDCK cells (A), GFHK99 virus in DF-1 cells (B), MaMN99
834 virus in MDCK cells (C), NL09 virus in MDCK cells (D), GFHK99 virus in MDCK cells (E), and
835 GFHK99 virus in DF-1 cells (F). G) Fold change in amplification (maximum PFU output / PFU
836 input) relative to the MOI=0.01 PFU per cell condition is plotted for each virus-cell pairing. H) Burst

837 size, calculated as maximum PFU output / number of $HA^+$ cells detected by flow cytometry, is
838 plotted for each virus-cell pairing tested in the higher MOI range. MOIs shown are in units of PFU
839 per cell, as determined in MDCK cells. Error bars represent mean ± standard error.
840
841 **Figure 3. Coinfection enhances GFHK99 vRNA synthesis in a dose and host dependent**
842 **manner.** Cells were coinfected with WT virus and increasing doses of VAR virus. WT virus MOI
843 was 0.05 PFU per cell in NHBE cells and 0.005 PFU per cell in all other cell types. The fold change
844 in WT vRNA copy number, relative to that detected in the VAR virus, is plotted for NL09 virus in
845 MDCK and NHBE cells (A), MaMN99 virus in MDCK and duck embryo (DE) cells (B), dkHK78
846 virus in MDCK, NHBE, and DF-1 cells (C), GFHK99 virus in MDCK, NHBE, and DF-1 cells (D)
847 and QaHK88 virus in MDCK, NHBE, and DF-1 cells (E). n=3 cell culture dishes per condition.
848 Error bars represent mean ± standard deviation.
849
850 **Figure 4. Coinfection and reassortment of chimeric viruses reveal a major role for the viral**
851 **PA gene segment.** Reverse genetics was used to place one or more genes from GFHK99 virus
852 into a MaMN99 background. Coinfections with homologous WT and VAR strains were performed
853 in MDCK cells as in Figure 1. The relationship between % cells HA positive and % cells dually HA
854 positive (A, B) and reassortment levels (C, D) are shown for each genotype. Experimental results
855 are compared to a theoretical prediction based on Poisson statistics and in which singly infected
856 and multiply infected cells have equivalent burst sizes (Prediction). Clustering analysis of the
857 regression models shown in (A-D) is used to partition the behavior of each chimeric genotype into
858 one of two clusters, denoting closer similarity to GFHK99 or MaMN99 (E). Yellow circles indicate
859 nodes with >95% bootstrap support. Data shown for GFHK99 and MaMN99 viruses are the same
860 as those displayed in Figure 1.
861

862 **Figure 5. High multiplicity of infection is needed for robust GFHK99 polymerase activity in**
863 **MDCK cells.** Dishes of MDCK or DF-1 cells (n=3) were infected with GFHK99 or MaMN99 virus
864 at low (0.5 RNA copies per cell) or high (3 HA-expressing units per cell) MOI. NS segment vRNA
865 and mRNA was quantified at the indicated time points (A–F). The average fold change from initial
866 (t=0) to peak RNA copy number is plotted for low MOI infections (G) and high MOI infections (H).
867 Error bars represent standard deviation. Significance was assessed by multiple unpaired t-tests
868 with correction for multiple comparisons using the Holm-Sidak method, with alpha = 5.0%. Each
869 row was analyzed individually, without assuming a consistent SD: *p < 0.05, **<0.01, ***<0.001.
870 ns = not significant.
871
872 **Figure 6. Homologous coinfecting virus boosts GFHK99 viral transcription in single cells**
873 **and reveals comparable rates of segment detection in MDCK and DF-1 cells.** DF-1 or MDCK
874 cells were infected with GFHK99 virus (left facet) at MOIs of 0.07, 0.2, 0.6, or 1.8 NP-expressing
875 units per cell, or a 1:1 mixture of GFHK99 WT and GFHK99 $mVAR_1$ viruses at four different total
876 MOIs (0.02, 0.07, 0.2, 0.6 NP-expressing units per cell) and a constant amount of GFHK99
877 $mVAR_2$ virus (0.1 PFU per cell in DF-1 cells, 1.0 PFU per cell in MDCK cells) (right facet). Violin
878 plots show the distribution of total viral RNA (A) or distinct viral genome segments (B) per cell in
879 each cell-MOI infection condition. Vertical lines denote the median of each distribution. UMI =
880 unique molecular identifier.
881
882 **Figure 7. Incomplete GFHK99 virus genomes are present but not sufficiently abundant to**
883 **account for observed reassortment in MDCK cells.** Incomplete viral genomes were quantified
884 experimentally by a single-cell assay which relies on the amplification of incomplete viral genomes
885 of GFHK99 WT virus (0.018 PFU per cell) by a genetically similar coinfecting virus, GFHK99
886 $VAR_2$. Based on the rate of detection of GFHK99 WT virus segments in this assay, the probability
887 that a given segment would be present and replicated in a singly infected MDCK cell is reported

as $P_P$. A) Summary of experimental $P_P$ data. n = 4 biological replicates, distinguished by color. Horizontal bars and shading represent mean ± standard deviation. Mean $P_{P,i}$ values for each segment are indicated at the bottom of the plot area. Average $P_P$ for each experiment was calculated as the geometric mean of the eight $P_{P,i}$ values, and the mean ± standard deviation of those four summary $P_P$ values is shown at the top of the plot area. B) Experimentally obtained $P_{P,i}$ values in A were used to parameterize a computational model[18]. Levels of reassortment predicted using the experimentally determined parameters are shown with colors corresponding to points in (A). Levels of reassortment predicted if $P_P$=1.0 are shown with the dashed line. Observed reassortment of GFHK99 WT and VAR viruses in MDCK cells are shown with blue circles. Observed reassortment of GFHK99 WT and VAR viruses in DF-1 cells are shown with pink circles. Observed data are the same as those plotted in Figure 1.

**Figure 8. Model: complementation of incomplete viral genomes is necessary but not sufficient for robust progeny production from mammalian cells infected with GFHK99 virus.** Cells infected with single virions often replicate incomplete viral genomes and therefore do not produce viral progeny (A). In mammalian cells, complementation of incomplete viral genomes through coinfection may allow progeny production (B), but robust viral yields require the delivery of additional genomes to the cell, beyond the levels needed for complementation (C). Horizontal bars within cells represent viral gene segments successfully delivered and replicated.

## References


1 Leeks, A., Sanjuan, R. & West, S. A. The evolution of collective infectious units in viruses. *Virus Res* **265**, 94-101, doi:10.1016/j.virusres.2019.03.013 (2019).

2 Brooke, C. B. Population Diversity and Collective Interactions during Influenza Virus Infection. *J Virol* **91**, doi:10.1128/JVI.01164-17 (2017).

3 Sanjuan, R. Collective Infectious Units in Viruses. *Trends Microbiol* **25**, 402-412, doi:10.1016/j.tim.2017.02.003 (2017).

4 Santiana, M. *et al.* Vesicle-Cloaked Virus Clusters Are Optimal Units for Inter-organismal Viral Transmission. *Cell Host Microbe* **24**, 208-220 e208, doi:10.1016/j.chom.2018.07.006 (2018).

917 5 Chen, Y. H. *et al.* Phosphatidylserine vesicles enable efficient en bloc transmission of
918 enteroviruses. *Cell* **160**, 619-630, doi:10.1016/j.cell.2015.01.032 (2015).
919 6 Erickson, A. K. *et al.* Bacteria Facilitate Enteric Virus Co-infection of Mammalian Cells and Promote
920 Genetic Recombination. *Cell Host Microbe* **23**, 77-88 e75, doi:10.1016/j.chom.2017.11.007
921 (2018).
922 7 Andreu-Moreno, I. & Sanjuan, R. Collective Infection of Cells by Viral Aggregates Promotes Early
923 Viral Proliferation and Reveals a Cellular-Level Allee Effect. *Current biology : CB* **28**, 3212-
924 3219.e3214, doi:10.1016/j.cub.2018.08.028 (2018).
925 8 Cuevas, J. M., Duran-Moreno, M. & Sanjuan, R. Multi-virion infectious units arise from free viral
926 particles in an enveloped virus. *Nat Microbiol* **2**, 17078, doi:10.1038/nmicrobiol.2017.78 (2017).
927 9 Cifuentes-Munoz, N., Dutch, R. E. & Cattaneo, R. Direct cell-to-cell transmission of respiratory
928 viruses: The fast lanes. *PLoS Pathog* **14**, e1007015, doi:10.1371/journal.ppat.1007015 (2018).
929 10 Lawrence, D. M. *et al.* Measles virus spread between neurons requires cell contact but not CD46
930 expression, syncytium formation, or extracellular virus production. *J Virol* **74**, 1908-1918,
931 doi:10.1128/jvi.74.4.1908-1918.2000 (2000).
932 11 McDonald, D. *et al.* Recruitment of HIV and its receptors to dendritic cell-T cell junctions. *Science*
933 **300**, 1295-1297, doi:10.1126/science.1084238 (2003).
934 12 Shirogane, Y., Watanabe, S. & Yanagi, Y. Cooperation between different RNA virus genomes
935 produces a new phenotype. *Nat Commun* **3**, 1235, doi:10.1038/ncomms2252 (2012).
936 13 Ciota, A. T., Ehrbar, D. J., Van Slyke, G. A., Willsey, G. G. & Kramer, L. D. Cooperative interactions
937 in the West Nile virus mutant swarm. *BMC Evol Biol* **12**, 58, doi:10.1186/1471-2148-12-58 (2012).
938 14 Xue, K. S., Hooper, K. A., Ollodart, A. R., Dingens, A. S. & Bloom, J. D. Cooperation between distinct
939 viral variants promotes growth of H3N2 influenza in cell culture. *Elife* **5**, e13974,
940 doi:10.7554/eLife.13974 (2016).
941 15 Brooke, C. B., Ince, W. L., Wei, J., Bennink, J. R. & Yewdell, J. W. Influenza A virus nucleoprotein
942 selectively decreases neuraminidase gene-segment packaging while enhancing viral fitness and
943 transmissibility. *Proc Natl Acad Sci U S A* **111**, 16854-16859, doi:10.1073/pnas.1415396111
944 (2014).
945 16 Brooke, C. B. *et al.* Most influenza a virions fail to express at least one essential viral protein. *J*
946 *Virol* **87**, 3155-3162, doi:10.1128/JVI.02284-12 (2013).
947 17 Sun, J. & Brooke, C. B. Influenza A Virus Superinfection Potential Is Regulated by Viral Genomic
948 Heterogeneity. *MBio* **9**, doi:10.1128/mBio.01761-18 (2018).
949 18 Fonville, J. M., Marshall, N., Tao, H., Steel, J. & Lowen, A. C. Influenza Virus Reassortment Is
950 Enhanced by Semi-infectious Particles but Can Be Suppressed by Defective Interfering Particles.
951 *PLoS Pathog* **11**, e1005204, doi:10.1371/journal.ppat.1005204 (2015).
952 19 Jacobs, N. T. *et al.* Incomplete influenza A virus genomes occur frequently but are readiliy
953 complemented during localized viral spread. *Nature Communications* (2019).
954 20 Nayak, D. P. Defective interfering influenza viruses. *Annu Rev Microbiol* **34**, 619-644,
955 doi:10.1146/annurev.mi.34.100180.003155 (1980).
956 21 Von Magnus, P. Incomplete forms of influenza virus. *Adv Virus Res* **2**, 59-79 (1954).
957 22 Brooke, C. B. Biological activities of 'noninfectious' influenza A virus particles. *Future Virol* **9**, 41-
958 51, doi:10.2217/fvl.13.118 (2014).
959 23 Timm, C., Gupta, A. & Yin, J. Robust kinetics of an RNA virus: Transcription rates are set by genome
960 levels. *Biotechnology and bioengineering* **112**, 1655-1662, doi:10.1002/bit.25578 (2015).
961 24 Boulle, M. *et al.* HIV Cell-to-Cell Spread Results in Earlier Onset of Viral Gene Expression by
962 Multiple Infections per Cell. *PLoS Pathog* **12**, e1005964, doi:10.1371/journal.ppat.1005964
963 (2016).

964 25 Sanjuán, R. & Thoulouze, M.-I. Why viruses sometimes disperse in groups?(†). *Virus Evol* **5**,
965 vez014-vez014, doi:10.1093/ve/vez014 (2019).
966 26 Sigal, A. *et al.* Cell-to-cell spread of HIV permits ongoing replication despite antiretroviral therapy.
967 *Nature* **477**, 95-98, doi:10.1038/nature10347 (2011).
968 27 Webster, R. G., Hinshaw, V. S., Bean, W. J., Jr., Turner, B. & Shortridge, K. F. Influenza viruses from
969 avian and porcine sources and their possible role in the origin of human pandemic strains. *Dev*
970 *Biol Stand* **39**, 461-468 (1977).
971 28 Wright, P. F., Neumann, G. & Kawaoka, Y. in *Fields Virology* Vol. 1 (ed D. M. & Howley Knipe, P.
972 M.) 1691-1740 (Lippincott-Raven, 2006).
973 29 Webster, R. G., Bean, W. J., Gorman, O. T., Chambers, T. M. & Kawaoka, Y. Evolution and ecology
974 of influenza A viruses. *Microbiol Rev* **56**, 152-179 (1992).
975 30 Webster, R. G., Shortridge, K. F. & Kawaoka, Y. Influenza: interspecies transmission and
976 emergence of new pandemics. *FEMS Immunol Med Microbiol* **18**, 275-279, doi:S0928-
977 8244(97)00058-8 [pii] (1997).
978 31 Taubenberger, J. K. & Morens, D. M. 1918 Influenza: the mother of all pandemics. *Emerg Infect*
979 *Dis* **12**, 15-22 (2006).
980 32 Viboud, C., Miller, M., Olson, D., Osterholm, M. & Simonsen, L. Preliminary Estimates of Mortality
981 and Years of Life Lost Associated with the 2009 A/H1N1 Pandemic in the US and Comparison with
982 Past Influenza Seasons. *PLoS Curr*, RRN1153, doi:k/-/-/35hpbywfdwl4n/8 [pii] (2010).
983 33 Long, J. S., Mistry, B., Haslam, S. M. & Barclay, W. S. Host and viral determinants of influenza A
984 virus species specificity. *Nat Rev Microbiol* **17**, 67-81, doi:10.1038/s41579-018-0115-z (2019).
985 34 Rajsbaum, R. *et al.* Species-specific inhibition of RIG-I ubiquitination and IFN induction by the
986 influenza A virus NS1 protein. *PLoS Pathog* **8**, e1003059, doi:10.1371/journal.ppat.1003059
987 (2012).
988 35 Manz, B. *et al.* Pandemic influenza A viruses escape from restriction by human MxA through
989 adaptive mutations in the nucleoprotein. *PLoS Pathog* **9**, e1003279,
990 doi:10.1371/journal.ppat.1003279

991 PPATHOGENS-D-12-02051 [pii] (2013).
992 36 Marshall, N., Priyamvada, L., Ende, Z., Steel, J. & Lowen, A. C. Influenza virus reassortment occurs
993 with high frequency in the absence of segment mismatch. *PLoS Pathog* **9**, e1003421,
994 doi:10.1371/journal.ppat.1003421 (2013).
995 37 Perez, D. R. *et al.* Role of quail in the interspecies transmission of H9 influenza A viruses: molecular
996 changes on HA that correspond to adaptation from ducks to chickens. *J Virol* **77**, 3148-3156,
997 doi:10.1128/jvi.77.5.3148-3156.2003 (2003).
998 38 Russell, A. B., Trapnell, C. & Bloom, J. D. Extreme heterogeneity of influenza virus infection in
999 single cells. *Elife* **7**, doi:10.7554/eLife.32303 (2018).
1000 39 Ramos, I. *et al.* Innate Immune Response to Influenza Virus at Single-Cell Resolution in Human
1001 Epithelial Cells Revealed Paracrine Induction of Interferon Lambda 1. *J Virol* **93**,
1002 doi:10.1128/JVI.00559-19 (2019).
1003 40 Cristobal Vera, J. *et al.* A common pattern of influenza A virus single cell gene expression
1004 heterogeneity governs the innate antiviral response to infection. *bioRxiv* (2019).
1005 41 Zheng, G. X. *et al.* Massively parallel digital transcriptional profiling of single cells. *Nat Commun* **8**,
1006 14049, doi:10.1038/ncomms14049 (2017).
1007 42 Lowen, A. C. It's in the mix: Reassortment of segmented viral genomes. *PLoS Pathog* **14**, e1007200,
1008 doi:10.1371/journal.ppat.1007200 (2018).
1009 43 Jagger, B. W. *et al.* An overlapping protein-coding region in influenza A virus segment 3 modulates
1010 the host response. *Science* **337**, 199-204, doi:10.1126/science.1222213 (2012).

1011 44 Te Velthuis, A. J. & Fodor, E. Influenza virus RNA polymerase: insights into the mechanisms of viral
1012 RNA synthesis. *Nat Rev Microbiol* **14**, 479-493, doi:10.1038/nrmicro.2016.87 (2016).
1013 45 Dias, A. *et al.* The cap-snatching endonuclease of influenza virus polymerase resides in the PA
1014 subunit. *Nature* **458**, 914-918, doi:nature07745 [pii]

1015 10.1038/nature07745 (2009).
1016 46 Fan, H. *et al.* Structures of influenza A virus RNA polymerase offer insight into viral genome
1017 replication. *Nature* **573**, 287-290, doi:10.1038/s41586-019-1530-7 (2019).
1018 47 Shi, M. *et al.* Evolutionary conservation of the PA-X open reading frame in segment 3 of influenza
1019 A virus. *J Virol* **86**, 12411-12413, doi:10.1128/JVI.01677-12 (2012).
1020 48 Gaucherand, L. *et al.* The Influenza A Virus Endoribonuclease PA-X Usurps Host mRNA Processing
1021 Machinery to Limit Host Gene Expression. *Cell reports* **27**, 776-792 e777,
1022 doi:10.1016/j.celrep.2019.03.063 (2019).
1023 49 Khaperskyy, D. A., Schmaling, S., Larkins-Ford, J., McCormick, C. & Gaglia, M. M. Selective
1024 Degradation of Host RNA Polymerase II Transcripts by Influenza A Virus PA-X Host Shutoff Protein.
1025 *PLoS Pathog* **12**, e1005427, doi:10.1371/journal.ppat.1005427 (2016).
1026 50 Butt, K. M. *et al.* Human infection with an avian H9N2 influenza A virus in Hong Kong in 2003. *J*
1027 *Clin Microbiol* **43**, 5760-5767, doi:43/11/5760 [pii]

1028 10.1128/JCM.43.11.5760-5767.2005 (2005).
1029 51 Peiris, M. *et al.* Human infection with influenza H9N2. *Lancet* **354**, 916-917,
1030 doi:S0140673699033115 [pii] (1999).
1031 52 Guan, Y. *et al.* H9N2 influenza viruses possessing H5N1-like internal genomes continue to circulate
1032 in poultry in southeastern China. *J Virol* **74**, 9372-9380 (2000).
1033 53 Guan, Y., Shortridge, K. F., Krauss, S. & Webster, R. G. Molecular characterization of H9N2
1034 influenza viruses: were they the donors of the "internal" genes of H5N1 viruses in Hong Kong?
1035 *Proc Natl Acad Sci U S A* **96**, 9363-9367 (1999).
1036 54 Lam, T. T. *et al.* The genesis and source of the H7N9 influenza viruses causing human infections in
1037 China. *Nature* **502**, 241-244, doi:10.1038/nature12515

1038 nature12515 [pii] (2013).
1039 55 Wu, A. *et al.* Sequential Reassortments Underlie Diverse Influenza H7N9 Genotypes in China. *Cell*
1040 *Host Microbe* **4**, 446-452, doi:S1931-3128(13)00298-9 [pii]

1041 10.1016/j.chom.2013.09.001 (2013).
1042 56 Gu, M., Xu, L., Wang, X. & Liu, X. Current situation of H9N2 subtype avian influenza in China. *Vet*
1043 *Res* **48**, 49-49, doi:10.1186/s13567-017-0453-2 (2017).
1044 57 Pusch, E. A. & Suarez, D. L. The Multifaceted Zoonotic Risk of H9N2 Avian Influenza. *Vet Sci* **5**, 82,
1045 doi:10.3390/vetsci5040082 (2018).
1046 58 Kayed, A. S. *et al.* Surveillance for avian influenza viruses in wild birds at live bird markets, Egypt,
1047 2014-2016. *Influenza Other Respir Viruses* **13**, 407-414, doi:10.1111/irv.12634 (2019).
1048 59 Xu, K. M. *et al.* The genesis and evolution of H9N2 influenza viruses in poultry from southern
1049 China, 2000 to 2005. *J Virol* **81**, 10389-10401, doi:10.1128/JVI.00979-07 (2007).
1050 60 White, M. C. & Lowen, A. C. Implications of segment mismatch for influenza A virus evolution. *J*
1051 *Gen Virol* **99**, 3-16, doi:10.1099/jgv.0.000989 (2018).
1052 61 Villa, M. & Lassig, M. Fitness cost of reassortment in human influenza. *PLoS Pathog* **13**, e1006685,
1053 doi:10.1371/journal.ppat.1006685 (2017).

1054 62 Chao, L., Tran, T. & Matthews, C. Muller's Ratchet and the Advantage of Sex in the Rna Virus 6.
1055 *Evolution; international journal of organic evolution* **46**, 289-299, doi:10.1111/j.1558-
1056 5646.1992.tb02038.x (1992).
1057 63 Froissart, R. *et al.* Co-infection weakens selection against epistatic mutations in RNA viruses.
1058 *Genetics* **168**, 9-19, doi:10.1534/genetics.104.030205 (2004).
1059 64 Novella, I. S., Reissig, D. D. & Wilke, C. O. Density-dependent selection in vesicular stomatitis virus.
1060 *J Virol* **78**, 5799-5804, doi:10.1128/JVI.78.11.5799-5804.2004 (2004).
1061 65 Wilke, C. O. & Novella, I. S. Phenotypic mixing and hiding may contribute to memory in viral
1062 quasispecies. *BMC Microbiol* **3**, 11, doi:10.1186/1471-2180-3-11 (2003).
1063 66 Danzy, S. *et al.* Mutations to PB2 and NP proteins of an avian influenza virus combine to confer
1064 efficient growth in primary human respiratory cells. *J Virol* **88**, 13436-13446,
1065 doi:10.1128/JVI.01093-14 (2014).
1066 67 Hoffmann, E., Neumann, G., Kawaoka, Y., Hobom, G. & Webster, R. G. A DNA transfection system
1067 for generation of influenza A virus from eight plasmids. **97**, 6108-6113,
1068 doi:10.1073/pnas.100133697 %J Proceedings of the National Academy of Sciences (2000).
1069 68 Schwartz, S. L. & Lowen, A. C. Droplet digital PCR: A novel method for detection of influenza virus
1070 defective interfering particles. *J Virol Methods* **237**, 159-165, doi:10.1016/j.jviromet.2016.08.023
1071 (2016).
1072 69 Perez, D. R., Webby, R. J., Hoffmann, E. & Webster, R. G. Land-based birds as potential
1073 disseminators of avian mammalian reassortant influenza A viruses. *Avian Dis* **47**, 1114-1117
1074 (2003).
1075 70 Song, H., Nieto, G. R. & Perez, D. R. A new generation of modified live-attenuated avian influenza
1076 viruses using a two-strategy combination as potential vaccine candidates. *J Virol* **81**, 9238-9248,
1077 doi:JVI.00893-07 [pii]

1078 10.1128/JVI.00893-07 (2007).
1079 71 Sorrell, E. M., Wan, H., Araya, Y., Song, H. & Perez, D. R. Minimal molecular constraints for
1080 respiratory droplet transmission of an avian-human H9N2 influenza A virus. *Proc Natl Acad Sci U*
1081 *S A* **106**, 7565-7570, doi:0900877106 [pii]

1082 10.1073/pnas.0900877106 (2009).
1083 72 Brown, J. D. *et al.* Intestinal excretion of a wild bird-origin H3N8 low pathogenic avian influenza
1084 virus in mallards (Anas Platyrhynchos). *Journal of wildlife diseases* **48**, 991-998, doi:10.7589/2011-
1085 09-280 (2012).
1086 73 Chen, H. *et al.* Partial and full PCR-based reverse genetics strategy for influenza viruses. *PLoS One*
1087 **7**, e46378, doi:10.1371/journal.pone.0046378

1088 PONE-D-12-21490 [pii] (2012).
1089 74 Matlin, K. S., Reggio, H., Helenius, A. & Simons, K. Infectious entry pathway of influenza virus in a
1090 canine kidney cell line. *J Cell Biol* **91**, 601-613, doi:10.1083/jcb.91.3.601 (1981).
1091 75 Yoshimura, A. & Ohnishi, S. Uncoating of influenza virus in endosomes. *J Virol* **51**, 497-504 (1984).
1092 76 Phipps, K. L. *et al.* Seasonal H3N2 and 2009 Pandemic H1N1 Influenza A Viruses Reassort Efficiently
1093 but Produce Attenuated Progeny. *J Virol* **91**, doi:10.1128/JVI.00830-17 (2017).
1094 77 Reed, L. J. & Muench, H. A SIMPLE METHOD OF ESTIMATING FIFTY PER CENT ENDPOINTS12.
1095 *American Journal of Epidemiology* **27**, 493-497, doi:10.1093/oxfordjournals.aje.a118408 (1938).
1096 78 Campbell, P. J. *et al.* The M segment of the 2009 pandemic influenza virus confers increased NA
1097 activity, filamentous morphology and efficient contact transmissibility to A/Puerto Rico/8/1934-
1098 based reassortant viruses. *J Virol*, doi:JVI.03607-13 [pii]

1099 10.1128/JVI.03607-13 (2014).
1100 79 Wittwer, C. T., Reed, G. H., Gundry, C. N., Vandersteen, J. G. & Pryor, R. J. High-resolution
1101 genotyping by amplicon melting analysis using LCGreen. *Clin Chem* **49**, 853-860 (2003).
1102 80 Richard, M., Herfst, S., Tao, H., Jacobs, N. T. & Lowen, A. C. Influenza A virus reassortment is
1103 limited by anatomical compartmentalization following co-infection via distinct routes. *J Virol*,
1104 doi:10.1128/JVI.02063-17 (2017).
1105 81 Simpson, E. H. Measurement of diversity. *Nature* **163**, 688-688 (1949).
1106 82 Hill, M. O. Diversity and evenness: a unifying notation and its consequences. *Ecology* **54**, 427-432
1107 (1973).
1108 83 Jost, L. Entropy and diversity. *Oikos* **113**, 363-375 (2006).
1109 84 Ward, J. Hierarchical Grouping to Optimize an Objective Function. *Journal of the American*
1110 *Statistical Association* **48**, doi:10.2307/2282967 (1963).
1111 85 Zhou, B. *et al.* Single-reaction genomic amplification accelerates sequencing and vaccine
1112 production for classical and Swine origin human influenza a viruses. *J Virol* **83**, 10309-10313,
1113 doi:JVI.01109-09 [pii]

1114 10.1128/JVI.01109-09 (2009).
1115 86 Drayman, N., Kler, S., Ben-nun-Shaul, O. & Oppenheim, A. Rapid method for SV40 titration. *J Virol*
1116 *Methods* **164**, 145-147, doi:10.1016/j.jviromet.2009.12.003 (2010).

1117

# Figure 1

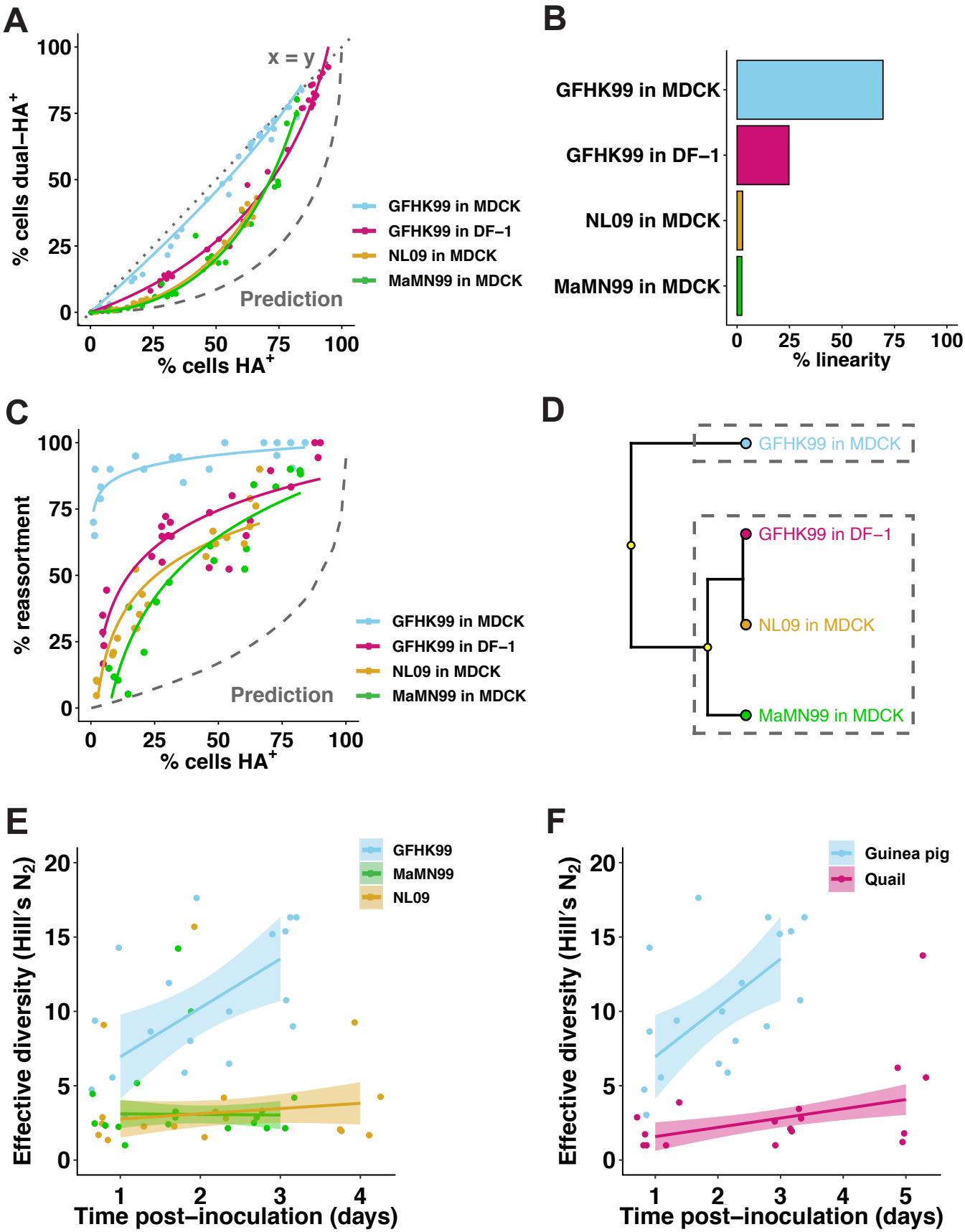
A
% cells dual–HA+
% cells HA+
x = y
Prediction
GFHK99 in MDCK
GFHK99 in DF–1
NL09 in MDCK
MaMN99 in MDCK
B
GFHK99 in MDCK
GFHK99 in DF–1
NL09 in MDCK
MaMN99 in MDCK
% linearity
C
% reassortment
% cells HA+
Prediction
GFHK99 in MDCK
GFHK99 in DF–1
NL09 in MDCK
MaMN99 in MDCK
D
GFHK99 in MDCK
GFHK99 in DF–1
NL09 in MDCK
MaMN99 in MDCK
E
Effective diversity (Hill's N2)
Time post–inoculation (days)
GFHK99
MaMN99
NL09
F
Effective diversity (Hill's N2)
Time post–inoculation (days)
Guinea pig
Quail

# Figure 2

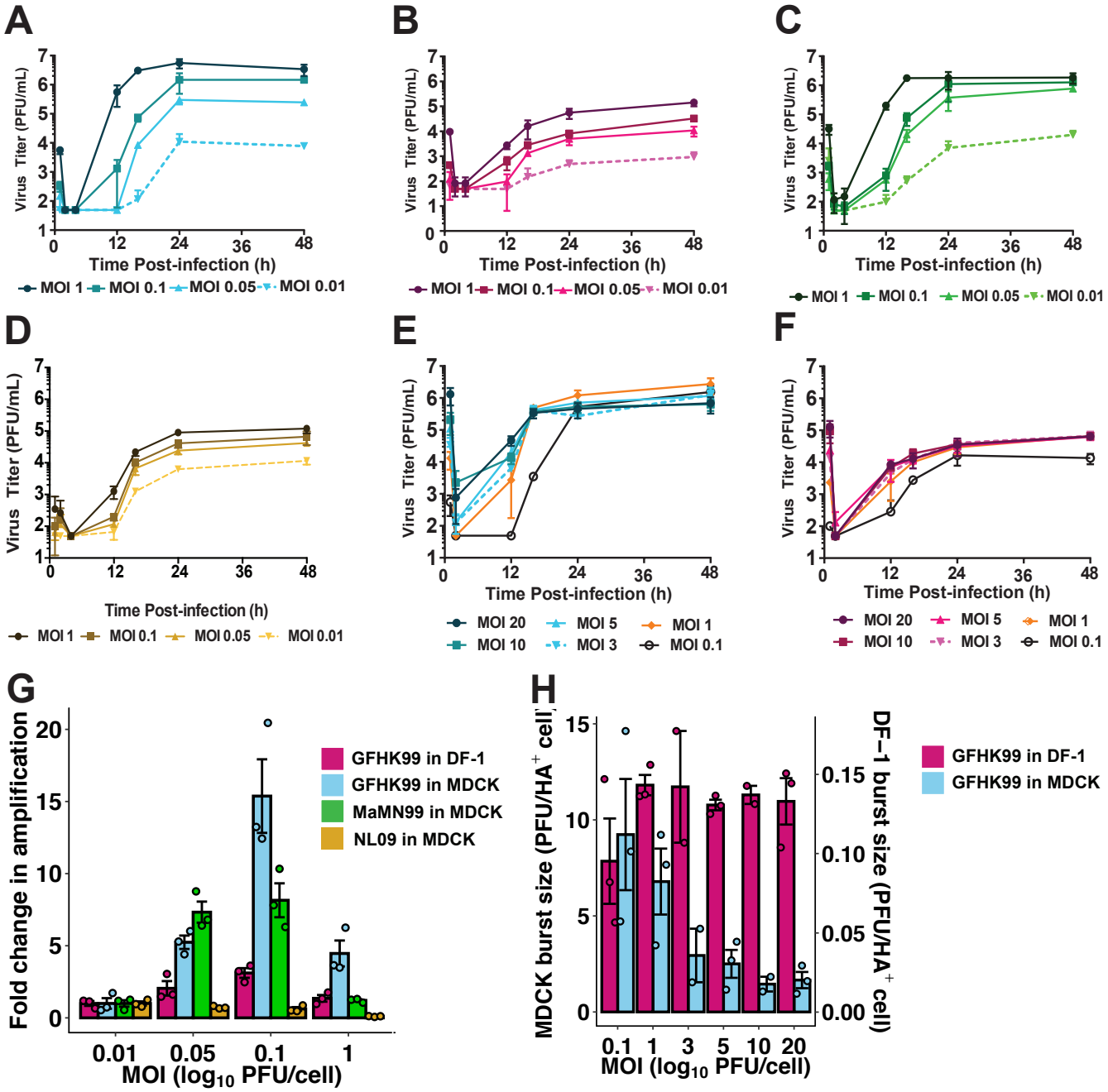
A
B
C
D
E
F
G
H
Virus Titer (PFU/mL)
Time Post-infection (h)
MOI 1
MOI 0.1
MOI 0.05
MOI 0.01
MOI 20
MOI 10
MOI 5
MOI 3
Fold change in amplification
MOI (log10 PFU/cell)
GFHK99 in DF-1
GFHK99 in MDCK
MaMN99 in MDCK
NL09 in MDCK
MDCK burst size (PFU/HA+ cell)
DF-1 burst size (PFU/HA+ cell)

# Figure 3

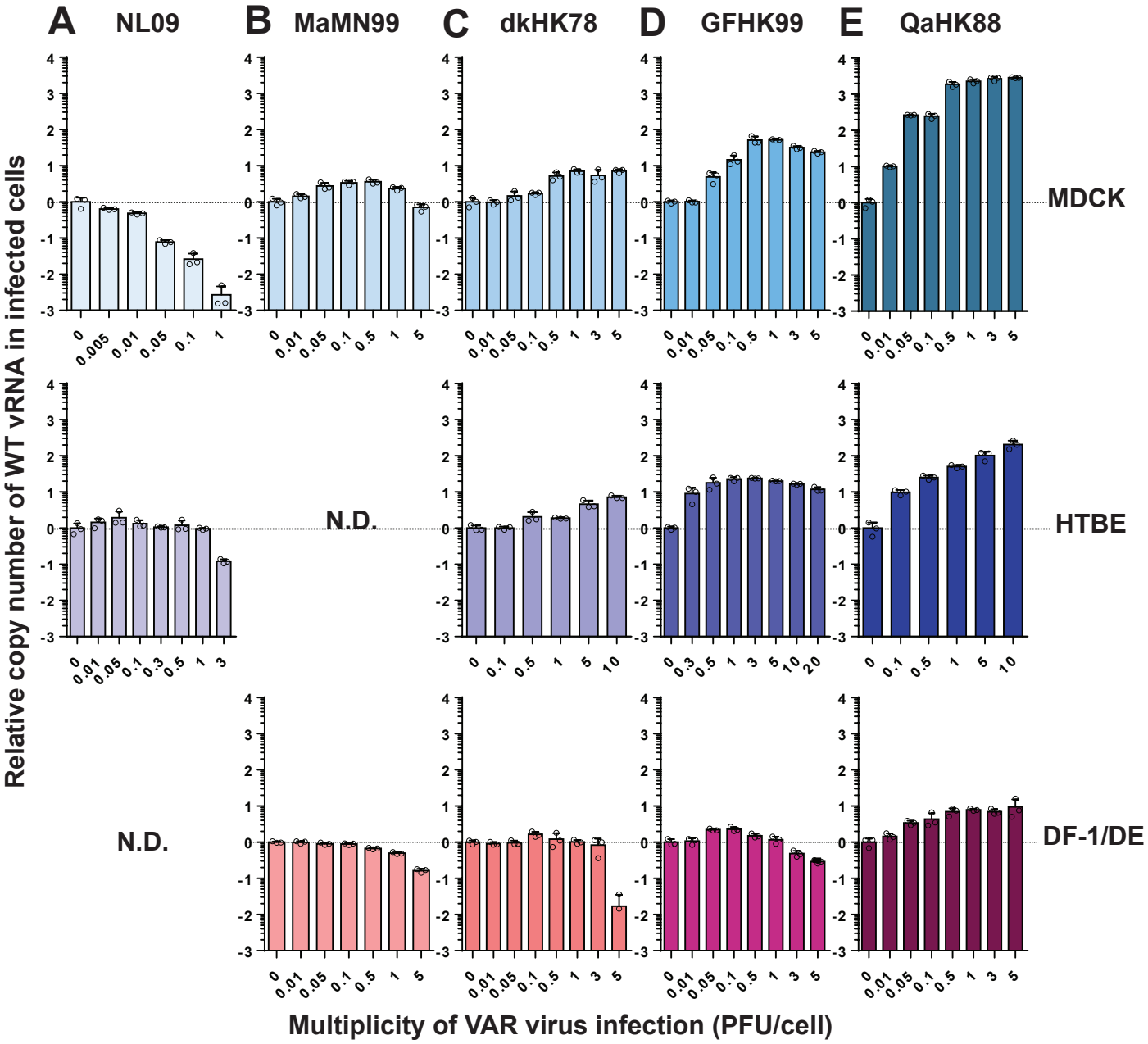
A NL09
B MaMN99
C dkHK78
D GFHK99
E QaHK88
MDCK
HTBE
DF-1/DE
N.D.
N.D.
Relative copy number of WT vRNA in infected cells
Multiplicity of VAR virus infection (PFU/cell)

# Figure 4

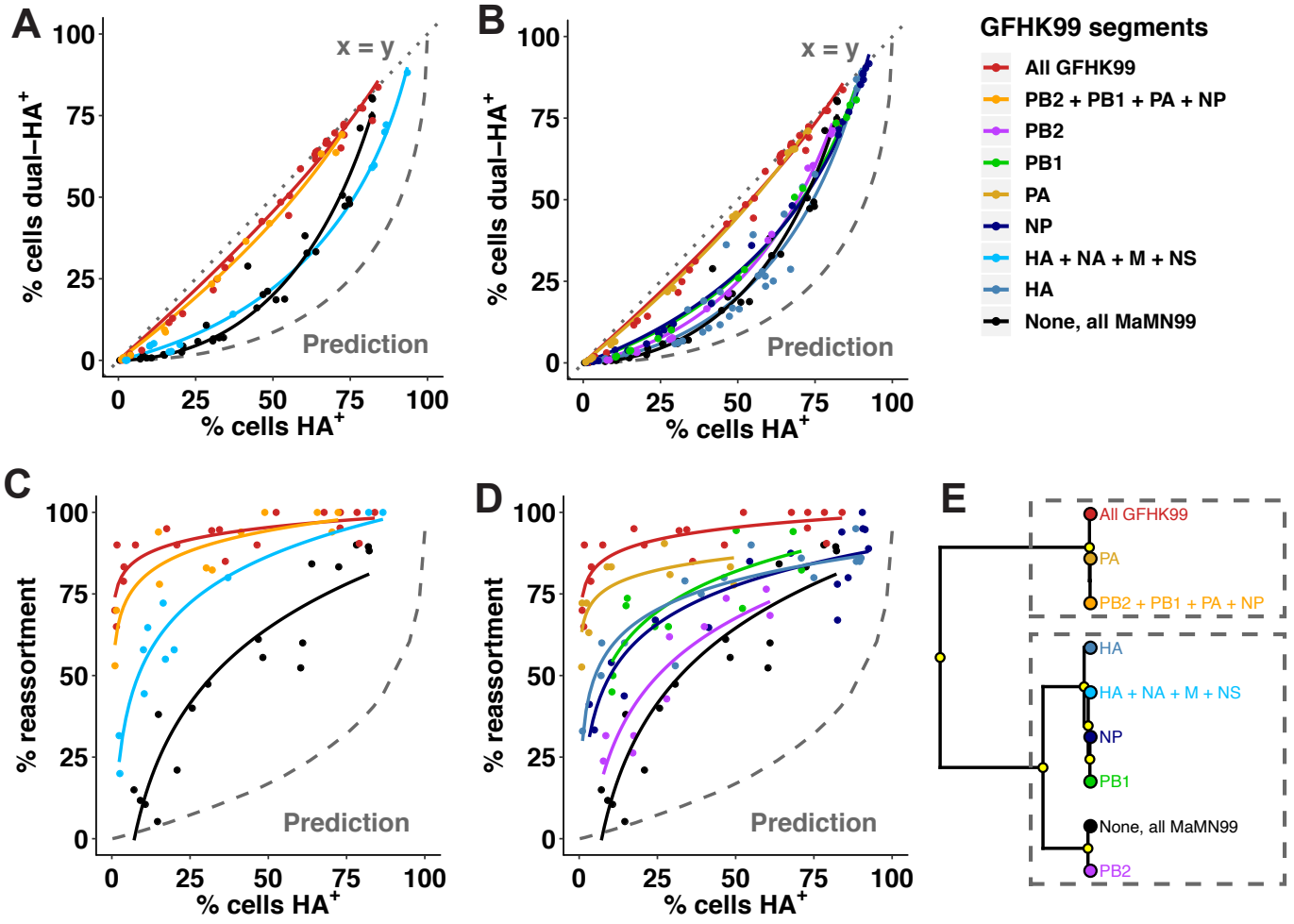
A
B
C
D
E
% cells dual–HA+
% cells HA+
% reassortment
x = y
Prediction
GFHK99 segments
All GFHK99
PB2 + PB1 + PA + NP
PB2
PB1
PA
NP
HA + NA + M + NS
HA
None, all MaMN99

# Figure 5

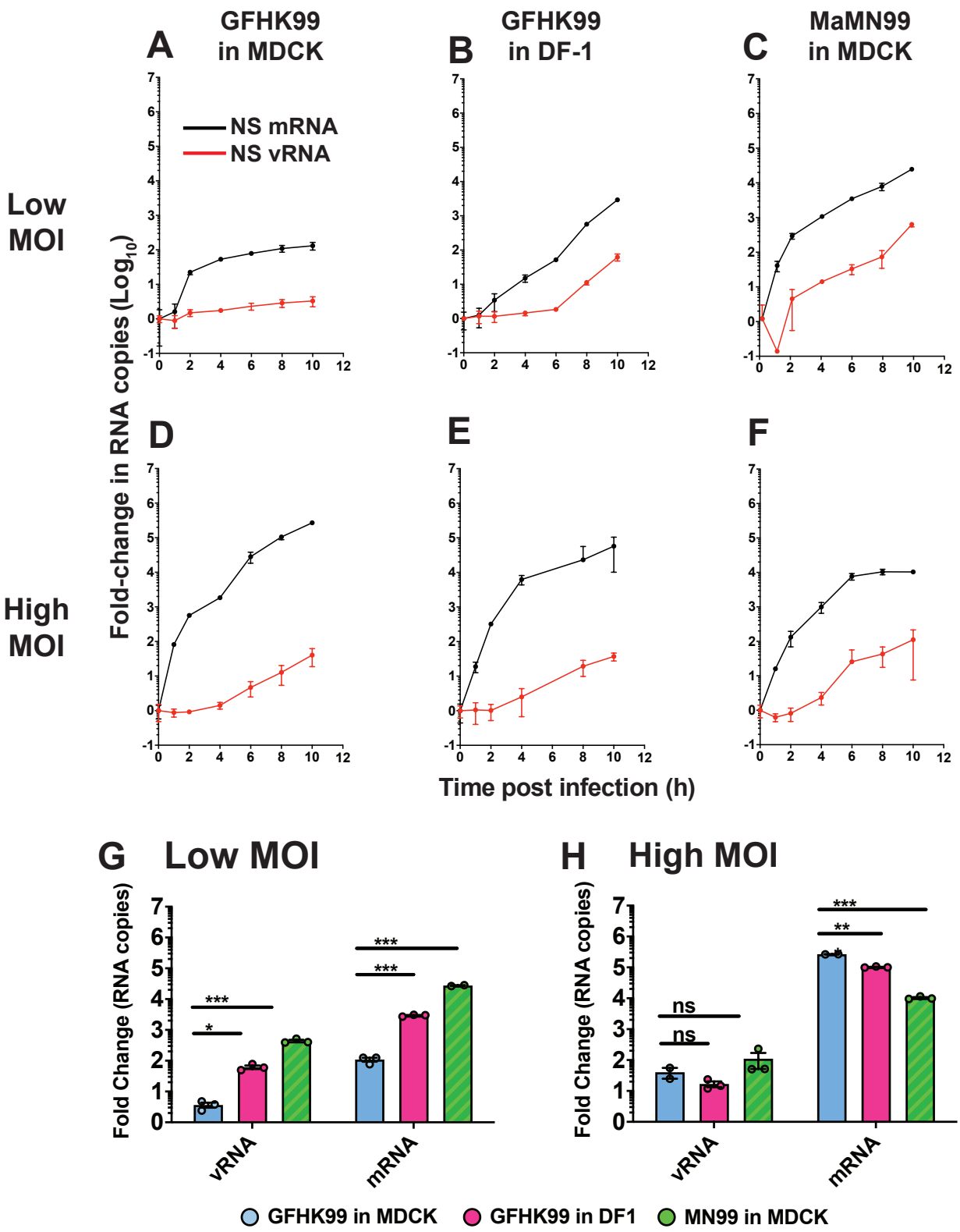
A
GFHK99 in MDCK
B
GFHK99 in DF-1
C
MaMN99 in MDCK
NS mRNA
NS vRNA
Low MOI
High MOI
D
E
F
Fold-change in RNA copies (Log10)
Time post infection (h)
G Low MOI
H High MOI
Fold Change (RNA copies)
***
*
***
***
ns
ns
***
**
vRNA
mRNA
GFHK99 in MDCK
GFHK99 in DF1
MN99 in MDCK

# Figure 6

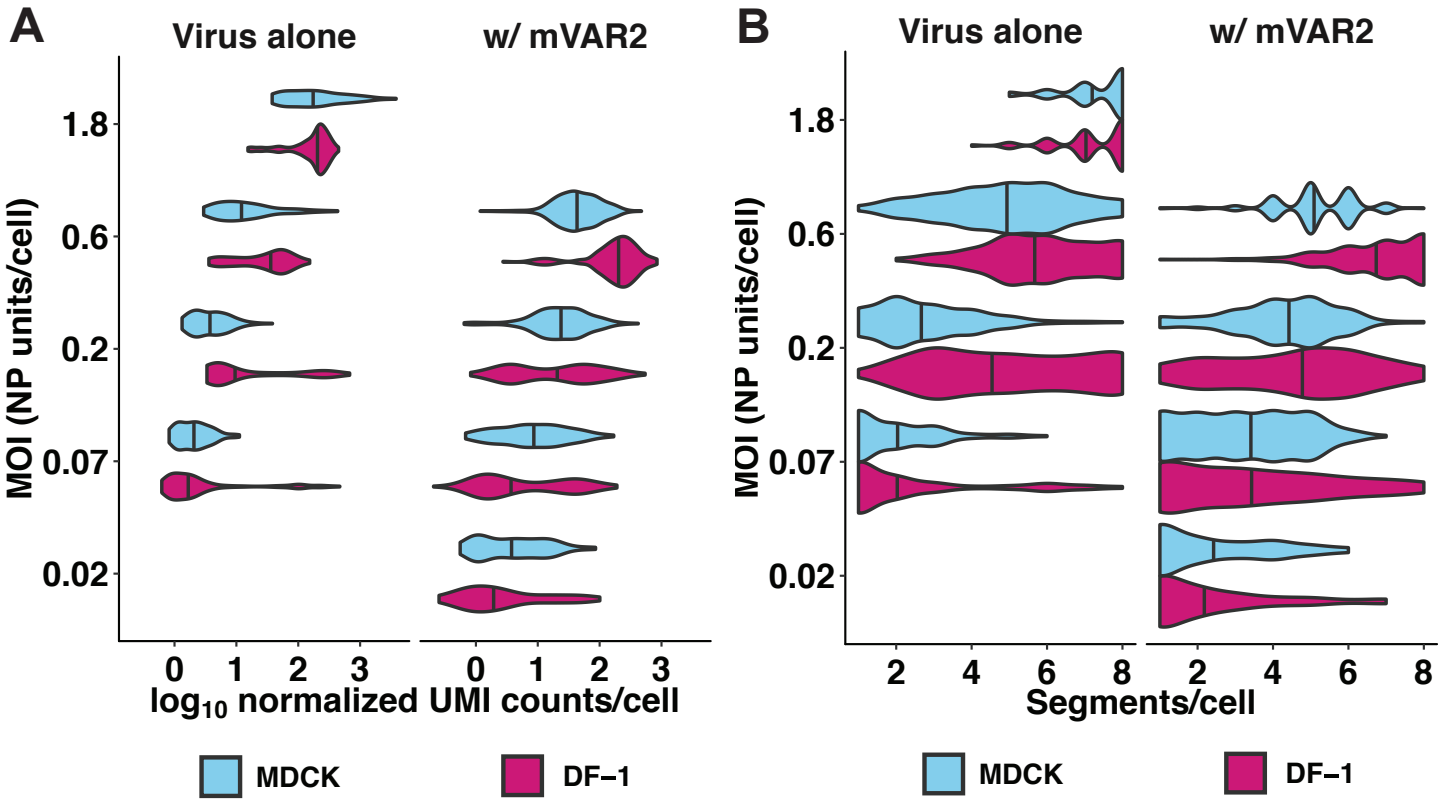
A
Virus alone
w/ mVAR2
MOI (NP units/cell)
1.8
0.6
0.2
0.07
0.02
0 1 2 3
0 1 2 3
log10 normalized UMI counts/cell
MDCK
DF–1
B
Virus alone
w/ mVAR2
MOI (NP units/cell)
1.8
0.6
0.2
0.07
0.02
2 4 6 8
2 4 6 8
Segments/cell
MDCK
DF–1

# Figure 7

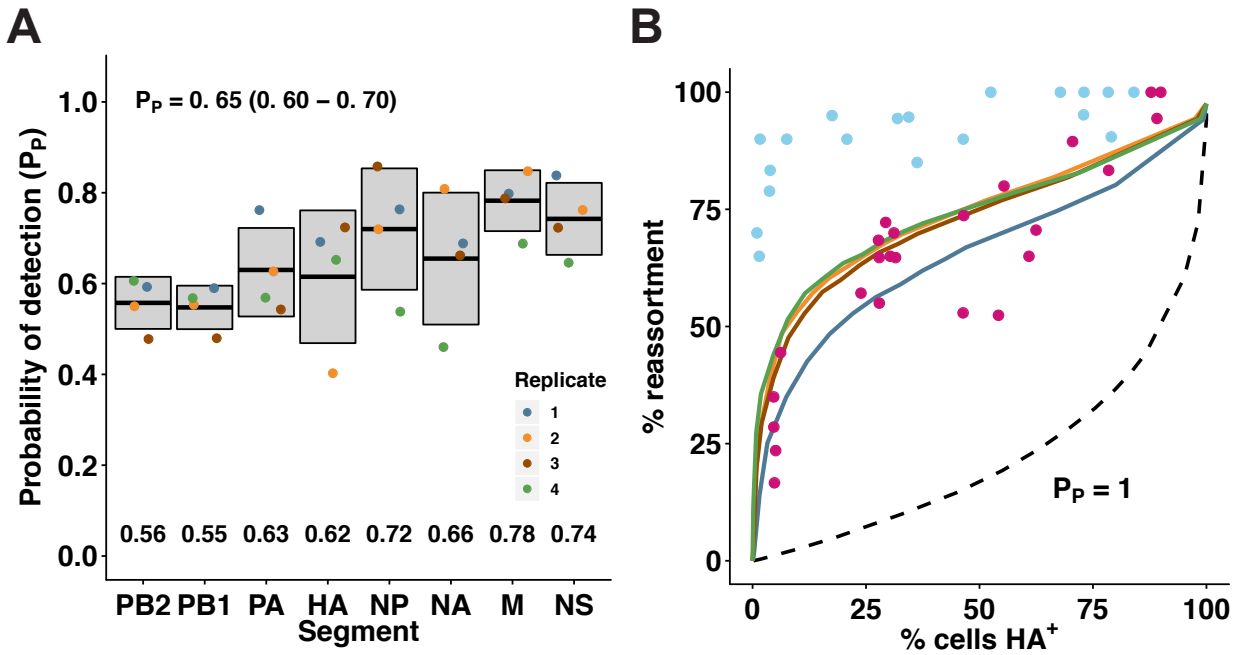
A
B
$P_P$ = 0. 65 (0. 60 – 0. 70)
Probability of detection ($P_P$)
1.0
0.8
0.6
0.4
0.2
0.0
Replicate
1
2
3
4
0.56 0.55 0.63 0.62 0.72 0.66 0.78 0.74
PB2 PB1 PA HA NP NA M NS
Segment
% reassortment
100
75
50
25
0
$P_P$ = 1
0 25 50 75 100
% cells HA+
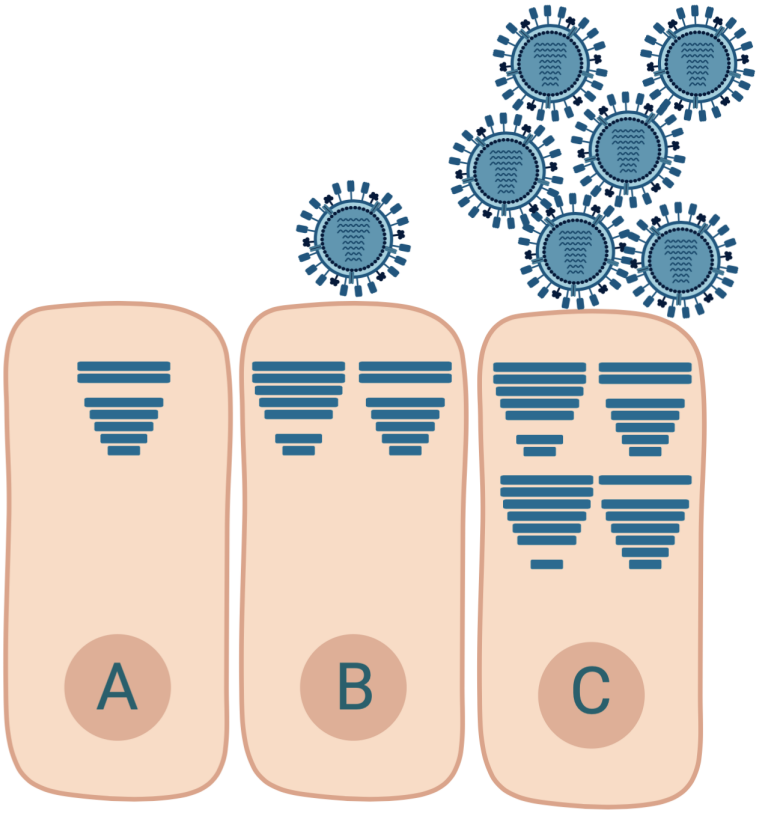
# Figure 8